nature chemical biology

Article

https://doi.org/10.1038/s41589-025-02037-5

Boolean logic-gated protein presentation through autonomously compiled molecular topology

Received: 30 May 2024

Accepted: 5 September 2025

Published online: 09 October 2025

Check for updates

Ryan Gharios[1,7], Murial L. Ross[2,7], Annabella Li[1], Shivani P. Kottantharayil[2], Jack Hoye[1] & Cole A. DeForest[1,2,3,4,5,6]

Stimulus-responsive materials have enabled advanced applications in biosensing, tissue engineering and therapeutic delivery. Although controlled molecular topology has been demonstrated as an effective route toward creating materials that respond to prespecified input combinations, prior efforts suffer from a reliance on complicated and low-yielding multistep organic syntheses that dramatically limit their utility. Harnessing the power of recombinant expression, we integrate emerging chemical biology tools to create topologically specified protein cargos that can be site-specifically tethered to and conditionally released from biomaterials following user-programmable Boolean logic. Critically, construct topology is autonomously compiled during expression through spontaneous intramolecular ligations, enabling direct and scalable synthesis of advanced operators. Using this framework, we specify protein release from biomaterials following all 17 possible YES/OR/AND logic outputs from input combinations of three orthogonal protease actuators, multiplexed delivery of three distinct biomacromolecules from hydrogels, five-input-based conditional cargo liberation and logically defined protein localization on or within living mammalian cells.

Programming stimulus responsiveness into biomaterials, living cells and biohybrid constructs represents an exciting frontier poised to galvanize many advanced bioengineering applications[1–3]. For instance, controlled presentation of biomolecules (for example, proteins, peptides, polysaccharides and nucleic acids) in or from materials holds direct applicability in therapeutic delivery[4,5], tissue engineering[6,7], organoid development[8,9] and the biomanufacturing of value-added chemicals[10]. Co-opting methods from organic and synthetic biobased chemistries[11–14], stimulus-responsive material platforms have been reported that sense and act upon diverse inputs including light[15–18], redox potential[19], enzyme[20,21] and pH[22]. While such approaches have largely transformed biomaterials from static to dynamic systems[23], the overwhelming majority of these platforms exhibit only single-input/single-output-type responses that dramatically limit their scope of use.

Recognizing that next-generation applications, including disease-triggered payload delivery[24,25] and analyte biosensing[26,27], would benefit tremendously from multistimulus responsiveness, truly 'smart' materials have been developed that transduce a set of environmental inputs into a functional output through user-specified Boolean logic[1]. Although logically defined biomolecule release has been accomplished using hydrogel–enzyme hybrids[28], degradable nanoparticles[29] and caged self-immolative polymers[30], existing strategies have been

[1]Department of Chemical Engineering, University of Washington, Seattle, WA, USA. [2]Department of Bioengineering, University of Washington, Seattle, WA, USA. [3]Department of Chemistry, University of Washington, Seattle, WA, USA. [4]Institute of Stem Cell & Regenerative Medicine, University of Washington, Seattle, WA, USA. [5]Molecular Engineering & Sciences Institute, University of Washington, Seattle, WA, USA. [6]Institute for Protein Design, University of Washington, Seattle, WA, USA. [7]These authors contributed equally: Ryan Gharios, Murial L. Ross. e-mail: profcole@uw.edu

https://doi.org/10.1038/s41589-025-02037-5

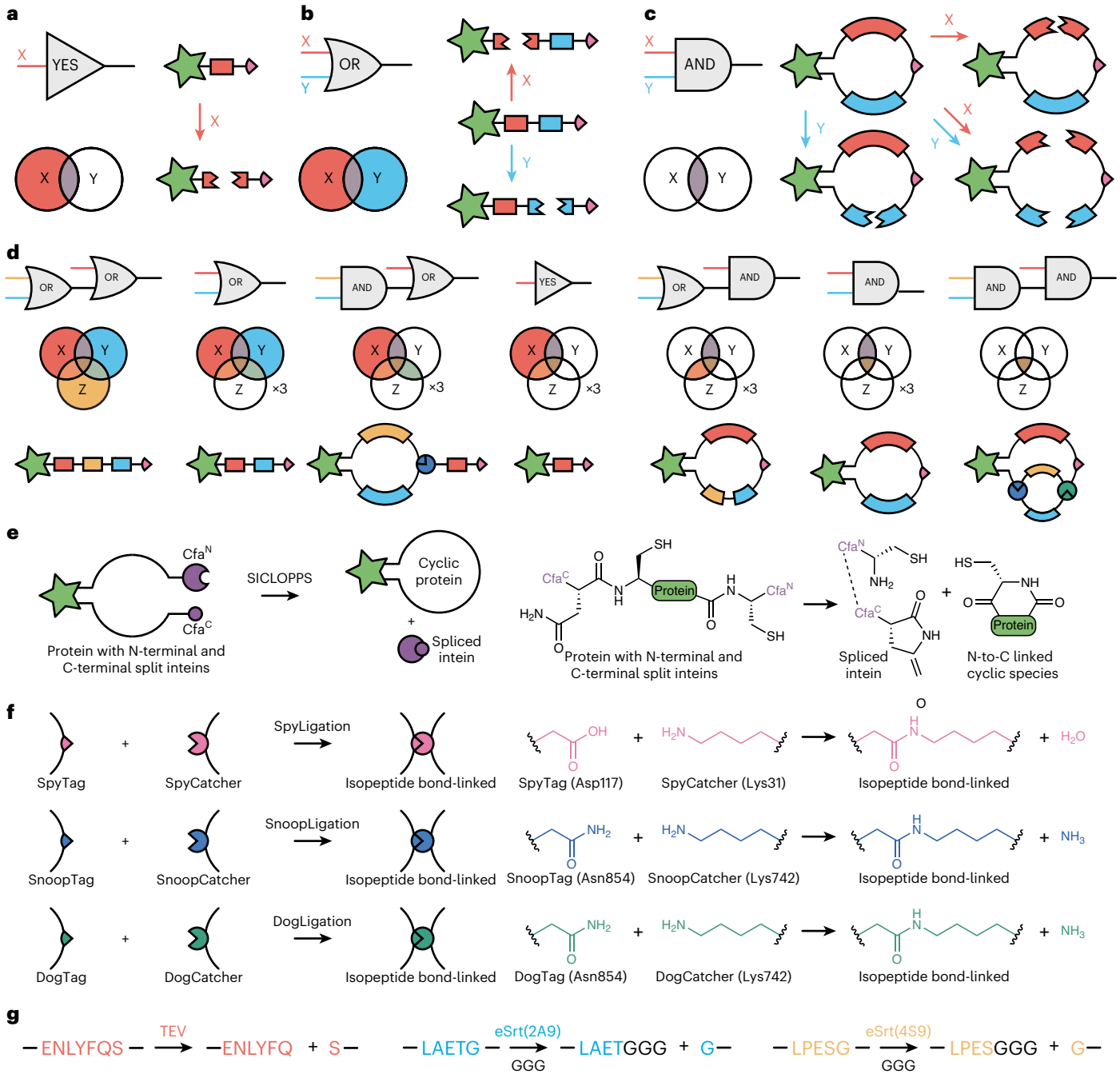

Fig. 1 | Autonomously compiled molecular topologies enable Boolean logic-based protein presentation. a, The YES-gated tether contains a single protease-responsive sequence (red). Introduction of the cognate protease cleaves this sequence, breaking the covalent linkage between the protein cargo (green star) and tethering motif (pink). **b**, The OR-gated tether contains two protease-responsive sequences (red and blue) connected in series. The introduction of either relevant protease cleaves the sequence, resulting in cargo release. **c**, The AND-gated tether contains two protease-responsive sequences (red and blue) connected in parallel. The introduction of one cognate protease cleaves one arm but does not fully sever the cycle. Simultaneous introduction of both proteases cleaves both arms, resulting in protein release. **d**, YES/OR/AND operators can be hierarchically layered to engineer higher-order logical responses. A total of 17 unique protein tethering topologies can be obtained through combination of the three base operations with three distinct protease actuators. Each region of the Venn diagrams displayed represents a unique combination of protease inputs and indicates whether the tether is predicted to cleave (colored) or remain intact (white). **e**, SICLOPPS provides a genetically encoded and near-traceless approach for the N-to-C cyclization of proteins based on intein *trans*-splicing. **f**, Tag/Catcher chemistries form isopeptide bonds between complementary protein modules through SpyLigation, SnoopLigation and DogLigation. **g**, Reactions depicting protease recognition of target sequence and subsequent cleavage: the recognition sequence ENLYFQ↓S is recognized and cleaved by the TEV protease, LAET↓G is recognized and cleaved by eSrtA(2A9) and LPES↓G is recognized and cleaved by eSrtA(4S9).

limited in their lack of generalizability, reliance on specific input chemistries and overall inability to elicit multiplexed operations. Toward imparting more modular Boolean biocomputability into materials, we recently demonstrated that molecular topology could be used to encode advanced environmental responsiveness[31–33]. Here, the linker between a biomolecule cargo and a stable material serves as an executable YES gate for programmable release when it contains a single degradable moiety, an OR gate (denoted with logic symbol ∨) when two

orthogonal cleavable moieties are included in series and an AND gate (denoted by logic symbol ∧) when two orthogonally scissile moieties are present in parallel (Fig. 1a–c). Importantly, logical gates can be expanded hierarchically to create advanced logical circuits responsive to several stimuli through nested YES/OR/AND operations (Fig. 1d). To date, such systems have been obtained through multistep organic reactions alongside solid-phase and solution-phase peptide synthesis—poorly scalable methods whose inherent complexity and low-yielding nature limit their implementation and potential for higher-ordered logical responses. Moreover, these systems cannot be synthesized and/or deployed within cells, precluding many applications from programming living function. Given these caveats, (bio)chemical strategies that permit one-step synthesis of logically releasable cargos would be profoundly enabling.

Toward expanding logical complexity, improving synthetic accessibility and exercising operations on/within living cells, we sought to identify generalizable biobased methods that enable the direct and facile assembly of topologically specified Boolean-responsive cargos. In this regard, we were drawn to the benefits of recombinant protein expression, augmented with recent advances in chemical biology. Recombinant polypeptides are highly monodisperse with a sequence defined by their encoding DNA, able to be produced at scale through well-established fermentation processes and amenable to the introduction of non-natural functionalities through semisynthesis[34] and/or genetic code expansion[35]. Furthermore, judicious use of engineered motifs permits the creation of heterodox protein architectures; proteins can be cyclized head to tail autocatalytically using split inteins (a method referred to as SICLOPPS[36,37]; Fig. 1e) or assembled into a variety of bespoke branched structures (for example, tadpoles, n-armed stars and H-shapes) using Tag/Catcher ligation chemistries (Fig. 1f)[38–40]. Although these advances can yield diverse protein topologies starting from simple, singular, plasmid blueprints[41–45], such methods have not previously been exploited for the creation of stimulus-responsive systems[46].

Here we introduce a modular chemical biology-based framework to autonomously compile proteins with defined molecular topology that can be site-specifically tethered to and conditionally released from biomaterials through nested Boolean operations. Using this template, we successfully demonstrate specification of protein release from biomaterials following all 17 possible YES/OR/AND logic outputs from input combinations of three orthogonal protease actuators, as well as the multiplexed delivery of three distinct biomacromolecules from a common hydrogel network through distinct logical operations. Further highlighting the expanded logical complexity enabled by these methods, we demonstrate control over protein liberation using a system that exercises biocomputation following a five-input Boolean-responsive operator circuit, as well as the ability to logically specify protein localization on and within living mammalian cells. Autonomous molecular compilation represents a powerful framework for biosynthesis and offers high specificity over biomolecule presentation in and from materials.

Results

Autonomous compilation of logic-gated proteins

Toward establishing design rules that functionally underlie our autonomous molecular compilation, we adopted mGreenLantern[47]—a monomeric green fluorescent protein variant recently evolved for enhanced brightness and expression levels—as a model protein cargo whose extent of release could be readily quantified through its fluorescence. Seeking to use cleavable moieties for protein release that are genetically encoded, we identified three protease actuators that operate on distinct peptide sequence substrates, sortase variants eSrtA(2A9) and eSrtA(4S9) evolved to recognize different pentapeptides (LAET↓G and LPES↓G, referred to as A and S, respectively)[48–50], alongside an evolved potyviral tobacco etch virus (TEV) protease (which acts upon sequence ENLYFQ↓S, referred to as T)[51,52], reasoning that the trio of actuators would exhibit no undesirable crosstalk (Fig. 1g). Having identified the mGreenLantern cargo and the three stimulus-labile moieties, we sought to recombinantly synthesize the 17 distinct logically responsive systems that exhaustively span all possible hierarchical YES/OR/AND combinations. To enable Ni-NTA-based immobilized metal affinity chromatography (IMAC) purification and covalent anchoring onto SpyCatcher-displaying materials[53], we installed both a 6×His tag and a SpyTag motif onto each protein regardless of the targeted logical operation.

With our design criteria established, we assembled the three base logical operators as follows: (1) YES gates (that is, A, S and T) were designed as routine constructs, harboring a protease-specific recognition sequence between the mGreenLantern cargo and the SpyTag anchor; (2) OR gates (that is, A∨S, A∨T and S∨T) followed a similar blueprint, whereby two distinct protease recognition sequences were installed in series between the cargo and material-tethering point; and (3) AND gates (that is, A∧S, A∧T and S∧T) were cyclized head to tail using a split Cfa intein by SICLOPPS[54,55]. To further bias the reaction toward complete splicing and eliminate possible byproducts, an SsrA tag was installed at the protein C terminus to mark all unspliced (that is, noncyclized) product for proteasomal degradation and clearance[56]. Plasmids encoding the nine possible YES-gated, OR-gated and AND-gated operators were transformed into BL21(DE3) *Escherichia coli*. Following conventional expression, proteins were purified by IMAC; cyclic constructs were further purified by size exclusion chromatography (SEC) to separate the target monocyclical constructs from higher-order macrocycle byproducts that can result from SICLOPPS (Supplementary Methods). In each case, desired proteins were obtained in good yield (YES and OR operators were produced at 30–50 mg L^{-1} of culture, whereas the AND operators had a final yield of approximately 20 mg L^{-1} of culture), as indicated by SDS–PAGE analysis and liquid chromatography–mass spectrometry (LC–MS) (Extended Data Fig. 1). Some higher-order macrocycles remained for AND-gated constructs following SEC (that is, ~15% of the S∧T and A∧T and ~25% for A∧S).

Heartened by our ability to recombinantly produce the base YES-type, OR-type and AND-type Boolean gates, each from a singular reading frame, we extended our methods to target higher-order logical operators responsive to distinct inputs. First, OR/(AND)-gated constructs (that is, A∨(S∧T), S∨(A∧T) and T∨(A∧S)) were designed to undergo macrocyclization through SnoopLigation[57,58], whereby installation of the SnoopCatcher motif at an internal site in the protein while keeping the SnoopTag at the N terminus leads to the creation of a bespoke branched structure that faithfully recreates the tadpole-like geometry necessary for the logical operation. Importantly, SnoopLigation and SpyLigation are fully orthogonal to each other, permitting

Fig. 2 | Autonomously assembled logic operators undergo preprogrammed cleavage from bead surfaces in response to actuator input combinations. **a**, SpyCatcher-functionalized magnetic beads can be decorated with different logical operators holding a SpyTag motif through SpyLigation. In this example, mGreenLantern-A is cleaved from the resin and solubilized in response to the $_A$ treatment. **b**, Supernatant fluorescence indicates logic-based release (here, to input $_A$). **c**, The response profiles of the YES-gated single-input tethers. **d**,**e**, The response profiles of the two-input OR-gated (**d**) and AND-gated (**e**) tethers. **f**–**i**, The response profiles of the three-input OR/(AND)-gated (**f**), AND/(OR)-gated (**g**), OR/OR-gated (**h**) and AND/AND-gated (**i**) tethers. Plot titles correspond to the protein tether identity. The *y* axis represents extent of protein release from bead surfaces as measured by supernatant fluorescence; the *x* axis indicates treatment conditions, wherein $_N$ indicates no treatment, $_A$ indicates eSrtA(2A9), $_S$ indicates eSrtA(4S9) and $_T$ indicates TEV. Green bars indicate conditions expected to yield tether cleavage, whereas red bars indicate conditions not expected to yield release. Error bars correspond to ±1 s.d. about the mean with propagated uncertainties for $n = 3$ experimental replicates.

https://doi.org/10.1038/s41589-025-02037-5

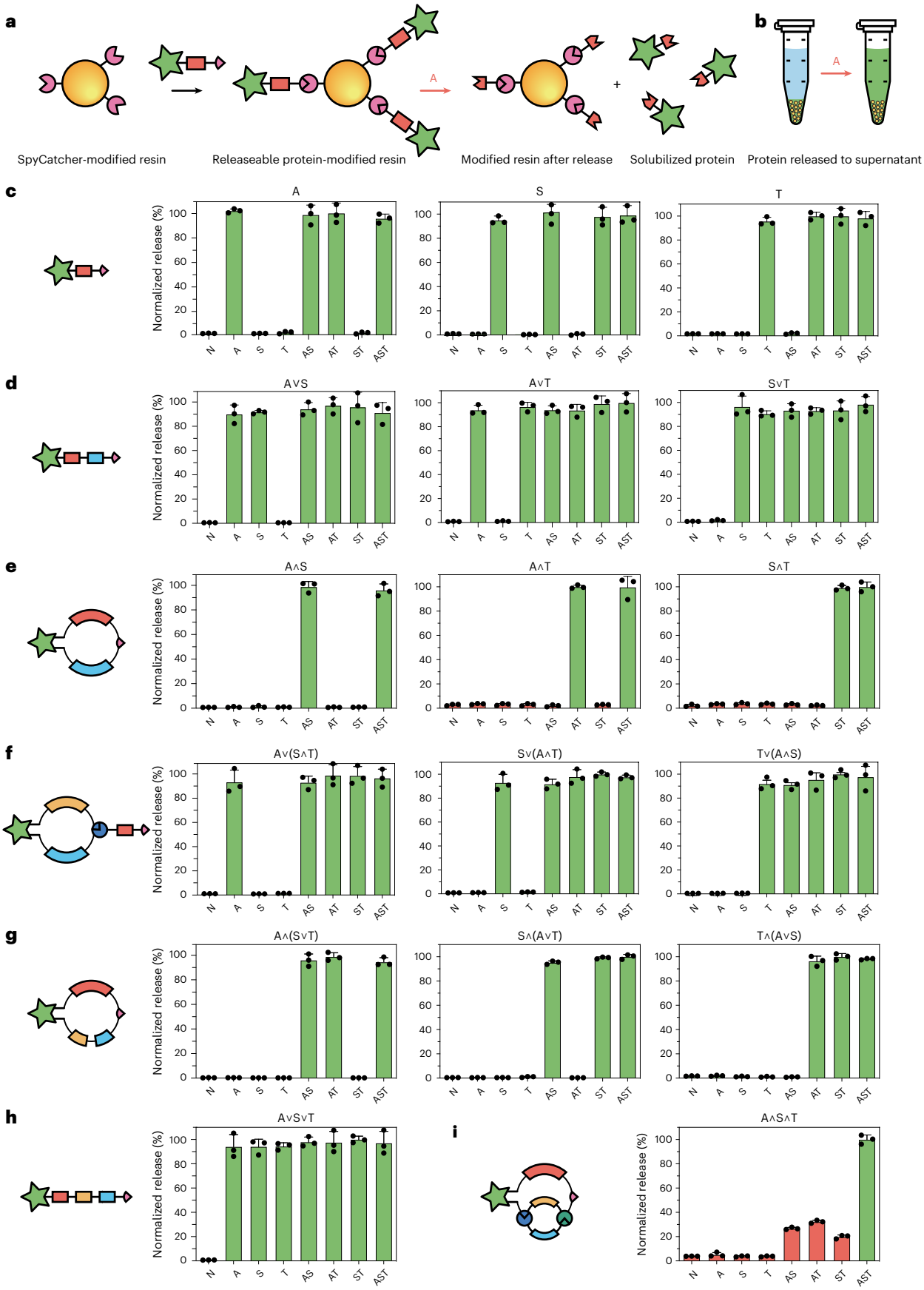

https://doi.org/10.1038/s41589-025-02037-5

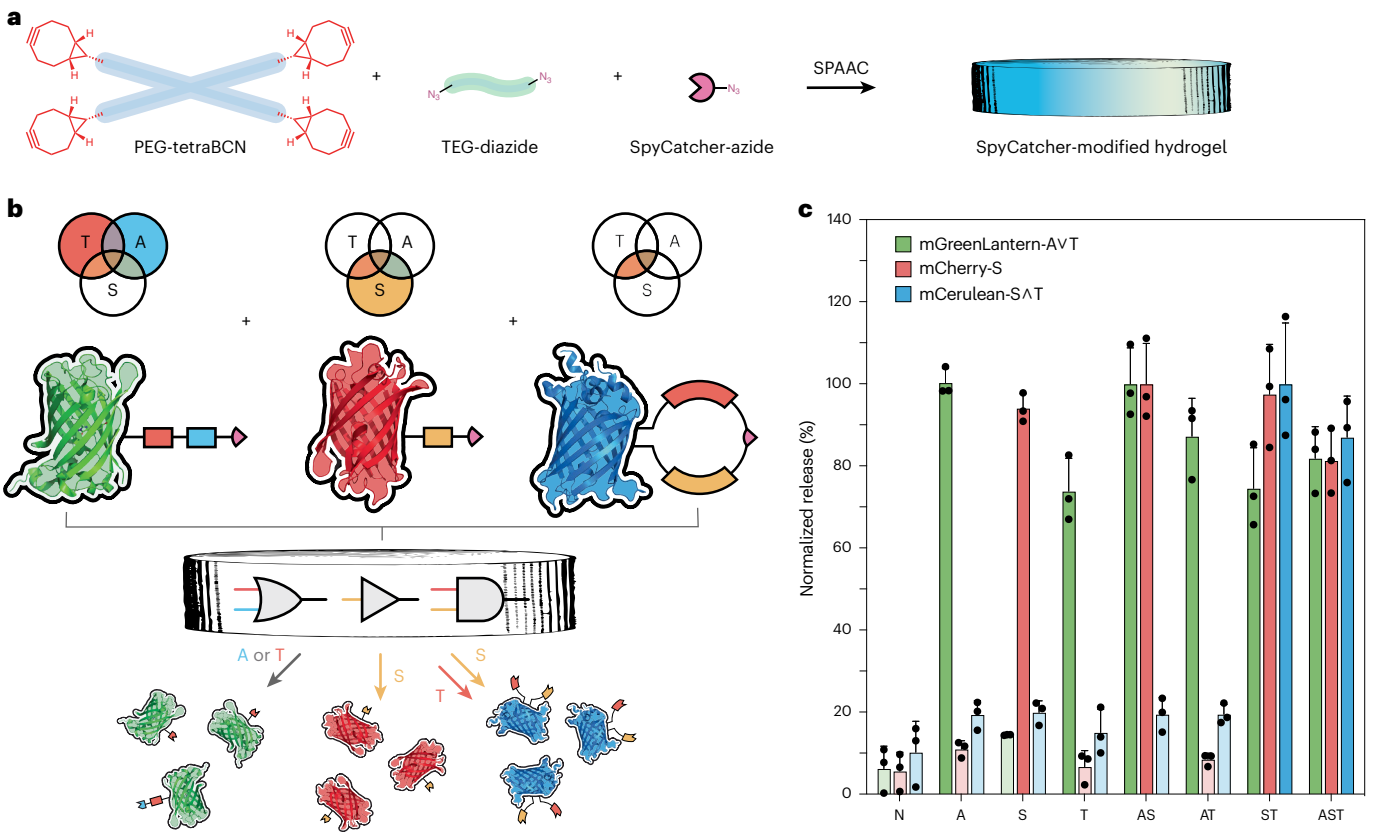

Fig. 3 | Autonomously compiled molecular topologies enable the multiplexed and independently triggered release of distinct proteins from a hydrogel network. a, PEG-tetraBCN, TEG-diazide and SpyCatcher-azide ligated to SpyTagged proteins of interest react by SPAAC to form functionalized hydrogels. **b**, mGreenLantern-A∨T, mCherry-S and mCerulean-S∧T are tethered homogenously into an underlying PEG network, each exhibiting a different logic-based release profile. **c**, Appropriate protein is released when the correct input combination is present. Fully colored bars (green for mGreenLantern, red for mCherry and blue for mCerulean) indicate conditions expected to yield protein release, whereas lightly colored bars denote conditions not expected to result in release. Error bars correspond to ±1 s.d. about the mean with propagated uncertainties for $n = 3$ experimental replicates.

complete chemical decoupling of payload configuration and anchoring, analogous to the use of orthogonal synthetic "click" chemistries for material synthesis[59]. Second, AND/(OR)-gated constructs (that is, A∧(S∨T), S∧(A∨T) and T∧(A∨S)) were assembled similarly to the dual-input AND structures, differing in that two of the cleavable sequences were expressed in series to one another and in parallel to the third. Third, the OR/OR-gated construct (that is, A∨S∨T) harbors the three protease substrate sequences expressed directly in series. Fourth, the AND/AND construct (that is, A∧S∧T) relies on two orthogonal Tag/Catcher ligations occurring in tandem to form a bicyclic protein cargo. Here, SnoopTag is installed at the cargo's N terminus and a DogTag[51] is installed at the C terminus, with their concomitant Catchers located internally in the expression frame. Plasmids encoding these eight remaining three-input systems were cloned, transformed into BL21(DE3) cells, expressed and purified by IMAC and SEC. All species were obtained with the expected molecular weights in good yield, as indicated by SDS–PAGE and LC–MS analysis (Extended Data Fig. 1). The OR/OR-gated and OR/(AND)-gated species were of high purity, while the AND/(OR)-gated constructs had good overall purity with <15% macrocycles present. The A∧S∧T target was correctly identified by whole-protein MS, although challenges separating the bicyclic and monocyclic species by SEC limited the final sample purity to ~75%.

Notably, the 17 distinct logically responsive proteins were autonomously compiled and obtained from singular plasmids by conventional fermentation and purification and characterized by a single researcher over the course of just a few weeks. In direct contrast to prior efforts reliant on organic synthesis and/or peptide chemistry, the reported approach features a rapid Design–Build–Test–Learn timeline that enables designs to be quickly sequence-optimized, structurally debugged and scaled up as needed.

Characterization of operator logical response in solution

With our core library in hand, we next sought to assay the 17 constructs' in-solution logical response to each of the eight possible input combinations of eSrtA(2A9) (denoted as $_A$), eSrtA(4S9) (denoted as $_S$) and TEV (denoted as $_T$) (Supplementary Fig. 1) at nonkinetically limited endpoints (Supplementary Figs. 2–4 and Supplementary Methods). As expected, changes in protein mass and/or topology gave rise to altered migration patterns[60–62], with full SDS–PAGE gels for all 17 logical operators and eight treatment conditions presented in Supplementary Fig. 5. Through gel densitometry, we quantified the extent of response for each protein to each input actuator set, demonstrating that our genetically encoded logical operators behaved as expected (Extended Data Fig. 2). Of note, we observed near-perfect responses with exceptionally high signal-to-noise ratios for 16 of the 17 operators, attributed to the simple yet meticulously engineered logical operators and the pristine targeting of orthogonal protease-driven actuation. Although small amounts of macrocycle contaminants were present in some samples, these did not interfere with logical operation or result in off-target release. Because of monocyclic impurities present in the A∧S∧T construct, gel densitometry analysis was not performed on the $_{AST}$-releasable cargo. The exhaustive validation of each possible construct demonstrates that complex biocomputation can be achieved with high fidelity through hierarchical nesting of simple YES/OR/AND logic gates.

https://doi.org/10.1038/s41589-025-02037-5

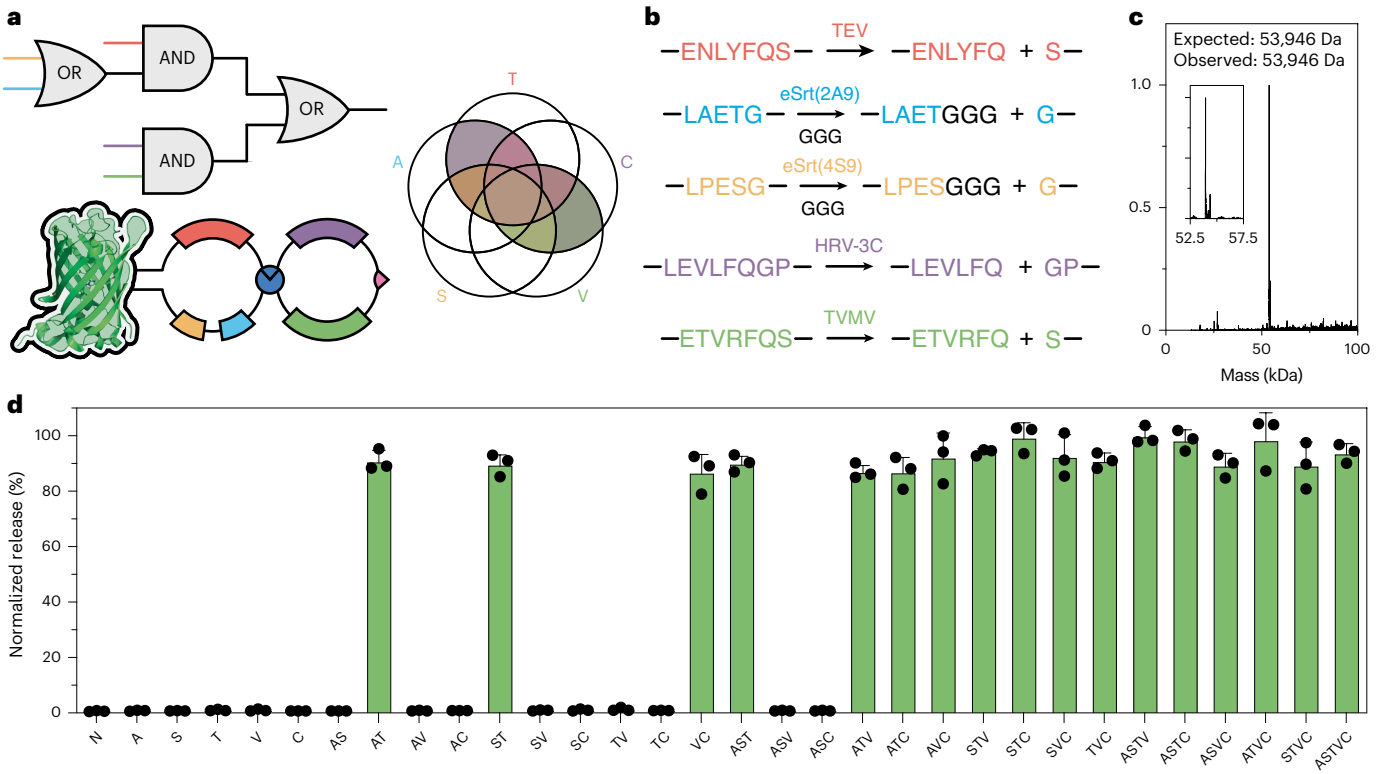

Fig. 4 | Genetic encodability enables seamless scale-up in logical response complexity. a, mGreenLantern-((A∨S)∧T)∨(C∧V) can be assembled on one expression frame and purified rapidly. Each region of the Venn diagrams displayed represents a unique combination of protease inputs and indicates whether the tether is predicted to cleave (colored) or remain intact (white). **b**, Reactions depicting protease recognition of target sequence and subsequent cleavage: the recognition sequence ENLYFQ↓S is recognized and cleaved by TEV, LAET↓G is recognized and cleaved by eSrtA(2A9), LPES↓G is recognized and cleaved by eSrtA(4S9), LEVLFQ↓GP is recognized and cleaved by HRV-3C and ETVRFQ↓S is recognized and cleaved by TVMV. **c**, mGreenLantern-((A∨S)∧T)∨(C∧V) is readily purified and obtained with the correct molecular mass. **d**, The response profiles of the five-input system. The *y* axis represents extent of protein release from bead surfaces as measured by supernatant fluorescence; the *x* axis indicates treatment conditions, wherein $_N$ indicates no treatment, $_A$ indicates eSrtA(2A9), $_S$ indicates eSrtA(4S9), $_T$ indicates TEV, $_V$ indicates TVMV and $_C$ indicates HRV-3C. Green bars indicate conditions expected to yield tether cleavage, whereas red bars indicate conditions expected to keep the tether uncleaved. Error bars correspond to ±1 s.d. about the mean with propagated uncertainties for $n = 3$ experimental replicates.

Characterization of operator logical response from magnetic bead surfaces

After molecularly validating construct behavior, we shifted our focus toward characterizing the stimulus responsiveness of the species in a materials' context[63]. Here we developed a magnetic bead-based assay enabling rapid interrogation of each protein's logical response to input actuator combinations, whereby supernatant fluorescence would indicate protease-driven mGreenLantern release from the solid support. Dibenzocyclooctyne (DBCO)-functionalized magnetic beads were uniformly decorated with a monofunctionalized SpyCatcher-azide protein by strain-promoted azide–alkyne cycloaddition (SPAAC)[64]. SpyCatcher-azide was obtained using genetic code expansion, wherein an azido-phenylalanine was site-specifically installed by amber suppression near the protein's C terminus (Supplementary Fig. 6 and Supplementary Methods) and served as a linker to immobilize each logic-releasable mGreenLantern protein to the supporting substrate. For each operator type, responsiveness to all eight input combinations involving $_A$, $_S$ and $_T$ was evaluated. Protein release was quantified by measuring supernatant fluorescence at nonkinetically limited endpoints following treatment (Fig. 2a,b). Consistent with the in-solution treatment assays, we observed the expected and near-perfect signal-to-noise release profiles for 16 of the 17 logical operators (Fig. 2c–i). The A∧S∧T system also yielded the desired response, in that there was much higher release accompanying the $_{AST}$ treatment compared to all other conditions but with ~25% undesired release in two-inputs (that is, $_{AS}$, $_{AT}$ and $_{ST}$) that we attributed to sample impurity (that is, the presence of monocyclic two-input responsive species); the ability to fully purify the logical species is essential in achieving perfect Boolean responsiveness, which may prove difficult for some higher-order constructs that rely on multiple cyclization chemistries. These logically advanced computational signatures for protein release will likely open doors for controlled drug delivery and biosensing.

Characterization of operator logical response from hydrogel matrices

We next sought to further extend the applicability of our method by programming biomacromolecule release from three-dimensional hydrogel networks, thus assessing the ability to trigger and multiplex signals through our autonomously compiled molecular topology-based approach. To do so, we first supplemented our protein toolkit by expressing and purifying two additional YES-gated fluorescent proteins that are spectrally separated from our starting $_A$-releasable mGreenLantern cargo (mGreenLantern-A, $\lambda_{exc.} = 495$ nm, $\lambda_{em.} = 525$ nm). Specifically, we constructed and purified an $_S$-releasable mCherry (mCherry-S, $\lambda_{exc.} = 580$ nm, $\lambda_{em.} = 610$ nm) and a $_T$-releasable mCerulean (mCerulean-T, $\lambda_{exc.} = 433$ nm, $\lambda_{em.} = 475$ nm) (Supplementary Fig. 2), both also containing a SpyTag motif for material anchoring and 6×His tag for purification. These species responded molecularly as expected to our exhaustive suite of potential inputs, indicated by SDS–PAGE analysis (Extended Data Fig. 3 and Supplementary Figs. 3 and 4). Poly(ethylene glycol) (PEG)-based hydrogels were synthesized through the SPAAC-based step-polymerization of a PEG-tetrabicyclononyne

https://doi.org/10.1038/s41589-025-02037-5

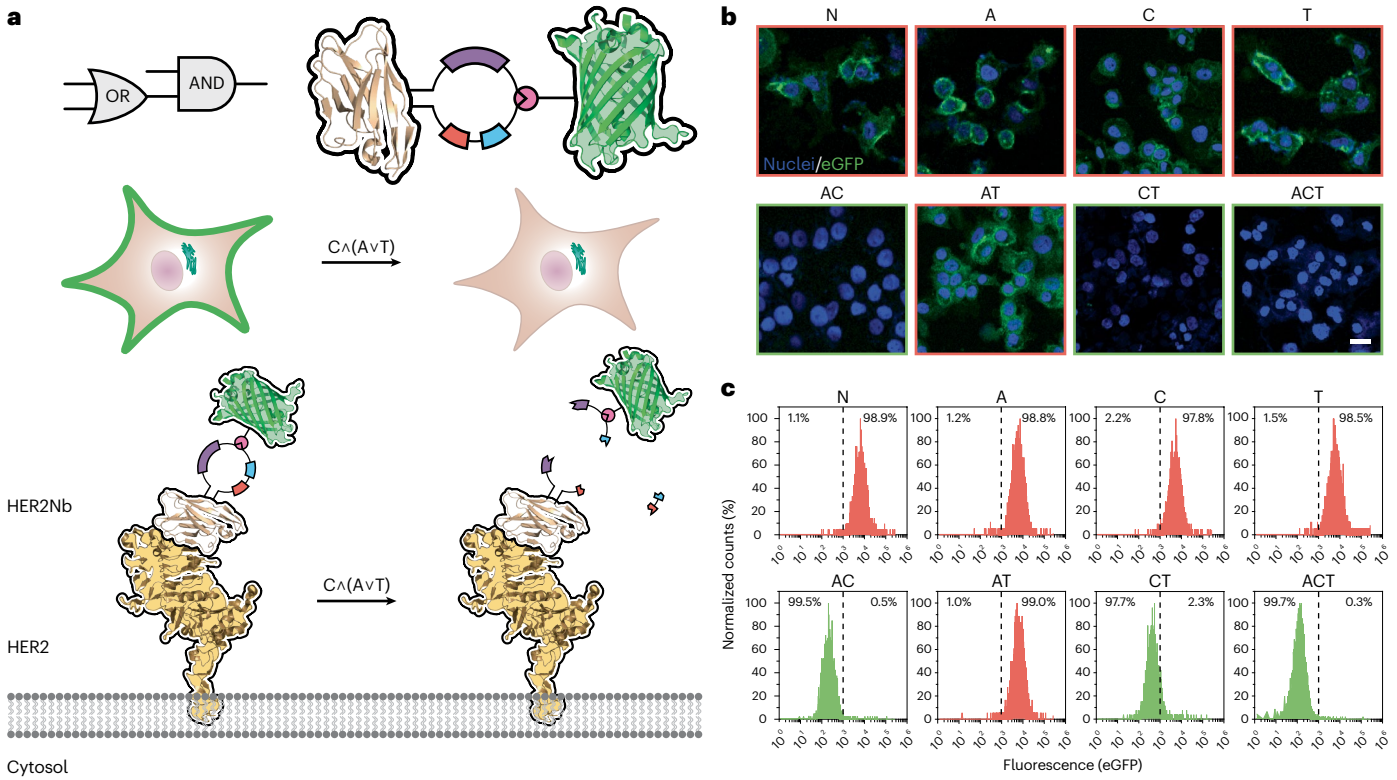

Fig. 5 | Boolean logic-based labeling of the mammalian extracellular membrane. a, HER2-expressing human breast cancer cells are tagged with an HER2Nb-C∧(A∨T)–eGFP, localizing a green fluorophore to the extracellular membrane through a nanobody–receptor interaction. An AND/(OR)-gated response of the HER2Nb-C∧(A∨T)–eGFP to eSrtA(2A9) ($_A$), TEV ($_T$) and HRV-3C ($_C$) before cell treatment prevents membrane labeling with eGFP. **b**, Fluorescent confocal microscopy indicates expected membrane labeling with eGFP (green), with nuclei counterstained with Hoechst 33342 (blue). Scale bar, 20 µm. **c**, Logically specified cell labeling was further confirmed by flow cytometry (10,000 events collected per condition). Conditions outlined in green or presented as a green histogram are those in which release is expected (that is, no cell labeling with eGFP); those in red indicate conditions not expected to yield release ($n = 1$ experimental replicates, independently for experiments in **b**,**c**).

(PEG-tetraBCN, M_n ~ 20 kDa) macromer and a triethylene glycol (TEG)-diazide[65] in the presence of a small amount of SpyCatcher-azide bound to mGreenLantern-A, mCherry-S and mCerulean-T through Spy-Ligation (Fig. 3a and Supplementary Methods). Such trifunctionalized hydrogels were subjected to each unique input combination involving $_A$, $_S$ and $_T$ and supernatant blue, green and red fluorescence was quantified to determine each individual protein release. Gratifyingly, the three proteins were released independently in the manner specified by their preprogrammed YES-gated input (Extended Data Fig. 4).

Looking to build on this initial success and benefit from the ease of assembly offered by our approach, we sought to go beyond the multiplexed release of YES operators and layer in different logical operators into the underlying matrix. Toward this end, we decorated our SpyCatcher-modified PEG hydrogels with mGreenLantern-A∨T, mCherry-S and an additionally designed and solution-characterized mCerulean-S∧T (Fig. 3b, Supplementary Figs. 7 and 8 and Extended Data Fig. 3). Following treatment with all possible actuator sets, we observed the release of each target biomacromolecule only in response to the appropriate cues or combinations thereof (Fig. 3c). Collectively, these studies establish a powerful route toward the creation of multi-input/multi-output materials.

Seamless scale-up of logical response and complexity through genetic encodability

Having successfully demonstrated the promise of autonomously compiled molecular topologies in three different contexts (that is, in solution, on surfaces and within hydrogel networks), we set out to leverage the intrinsic benefits of unsupervised biosynthesis to create a five-input-responsive (AND/(OR))OR(AND)-gated system, extending well beyond the biocomputational complexity achievable through other material approaches (Fig. 4a). Toward this goal, we identified two additional proteases expected to operate orthogonally to our existing set of inputs: the potyviral tobacco vein mottling virus (TVMV) protease (operating on substrate ETVRFQ↓S, referred to as V)[66] and the human rhinovirus 3C (HRV-3C) protease (recognizing LEVLFQ↓GP, denoted as C)[67] (Fig. 4b and Supplementary Fig. 1). Having identified our five input proteases, we sought to synthesize the mGreenLantern-((A∨S)∧T)∨(C∧V) protein, a design that would necessitate the compilation of a genetic blueprint into a bicyclic protein. To achieve such a logical operation, we adopted a recently pioneered 'assembly reaction' synergy approach, where motifs that assemble through fragment dimerization, catenation or similar mechanisms bring covalent chemistries (for example, Tag/Catcher ligations) into close proximity that drive reaction completion[68,69]. In our case, we reasoned that deploying SICLOPPS to cyclize a target protein would bring internal Tag and Catcher motifs into physical proximity, promoting complete ligation to create the pinch point-containing bicyclic protein. Using this methodology, our mGreenLantern-((A∨S)∧T)∨(C∧V) was generated solubly, in high purity (>95%) (Supplementary Fig. 9) and yield (5 mg L^{-1} of culture following IMAC/SEC) and with the expected molecular mass (Fig. 4c).

To validate the response signature of this logical construct, we immobilized mGreenLantern-((A∨S)∧T)∨(C∧V) onto SpyCatcher-functionalized magnetic beads and assessed release by supernatant fluorescence following treatment with each of the 32 potential actuator combination sets. We observed the expected

https://doi.org/10.1038/s41589-025-02037-5

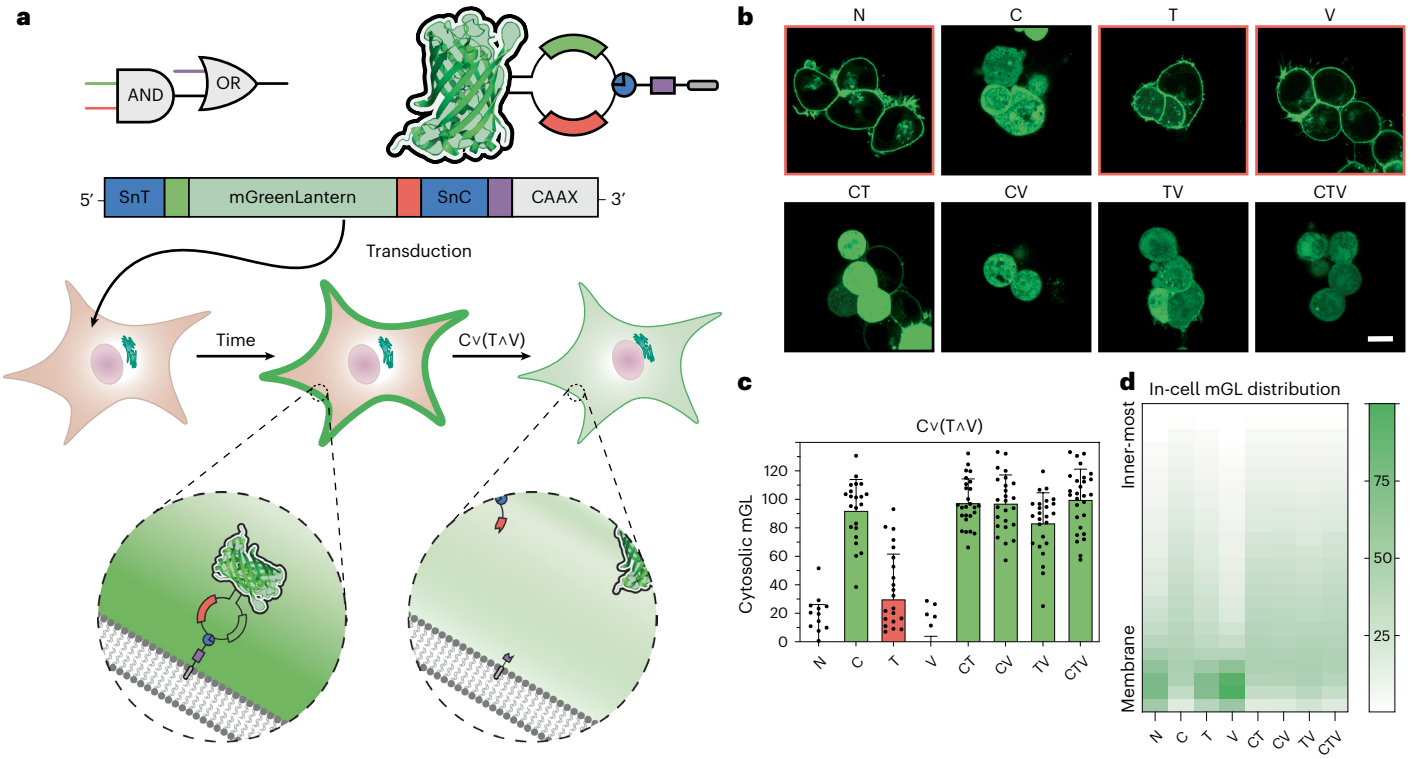

Fig. 6 | Autonomous compilation and logic-defined localization within mammalian cells. a, HEK293 cells are stably modified by lentiviral transduction to express an mGreenLantern-C∨(T∧V)−CAAX fusion that translocates to the intracellular plasma membrane. When cells are subsequently transfected with plasmids encoding for each of the eight relevant protease combinations, the fluorescent species is liberated from the cell membrane into the cytosol following an OR/(AND)-gated response to HRV-3C ($_C$), TEV ($_T$) and TVMV ($_V$). **b**, Fluorescent confocal microscopy indicates expected membrane labeling with mGreenLantern (green) following treatment. Scale bar, 10 µm. **c**,**d**, CellProfiler-based analysis of mGreenLantern intracellular positioning illustrates expected cytosolic presentation following $_C$, $_{CT}$, $_{CV}$, $_{TV}$ and $_{CTV}$ treatments. Conditions outlined or presented in green correspond to those in which release is expected (that is, cytosolic mGreenLantern); those in red indicate conditions not expected to yield release. Error bars correspond to ±1 s.d. about the mean ($n = 23_N$, $n = 22_C$, $n = 25_T$, $_{CV}$ and $_{TV}$, $n = 26_V$ and $_{CT}$ and $n = 28_{CTV}$ technical replicates).

anti-interferent five-input responsiveness, demonstrating protein release only in preprogrammed conditions with near-perfect signal-to-noise ratios (Fig. 4d and Supplementary Fig. 10). Excitingly, despite its functional complexity, this cargo was generated through routine recombinant methods and required no extensive debugging or recoding. Most promisingly, our studies suggest that the potential for even higher-order logical complexity is limited primarily by the number of orthogonally labile peptide motifs and fragment reconstitution chemistries that can be identified.

Logic-specified extracellular labeling of mammalian cells

Having established the ability to logically specify protein presentation on bead surfaces and within hydrogel biomaterials, we shifted our focus toward doing so in the context of living mammalian cells. After validating the cytocompatibility of the various input treatments (Supplementary Fig. 11), we created a C∧(A∨T)-gated nanobody—a single-domain antigen-binding protein derived from the heavy chain of an antibody—against the breast-cancer-associated human epidermal growth factor receptor type 2 (HER2)[70,71] (Fig. 5a). Here, the HER2 nanobody (HER2Nb) was fused to SpyTag through the cyclic C∧(A∨T) linkage and subsequently conjugated to a SpyCatcher-modified enhanced green fluorescent protein (eGFP) (Supplementary Methods). The resulting fusion construct (HER2Nb-C∧(A∨T)−eGFP) was obtained in good purity and expected molecular weight (Supplementary Figs. 12 and 13), responded as expected following in-solution treatment with the eight possible input combinations of $_A$, $_C$ and $_T$ (Supplementary Fig. 14) and selectively bound to the extracellular membrane of HER2-expressing SK-BR-3 cells (Supplementary Fig. 15).

Following the treatment of HER2Nb-C∧(A∨T)−eGFP with each of the eight relevant input combinations, samples were individually incubated with SK-BR-3 cells. After nuclear labeling with Hoechst 33342 and confocal imaging, fluorescent labeling of cells agreed with the AND/(OR)-specified logical operation; eGFP signal was not observed for cells treated with $_{AC}$, $_{CT}$ or $_{ACT}$, although all other conditions showcased extracellular labeling (Fig. 5b and Supplementary Methods). These findings were corroborated using flow cytometry, calculating the percentage of eGFP-positive cells for each protease condition (Supplementary Fig. 16). As expected, cells receiving the $_N$, $_A$, $_C$, $_T$ and $_{AT}$ treatments were fluorescently labeled (>97% eGFP$^+$), while those in which eGFP was proteolytically cleaved from HER2Nb (that is, $_{AC}$, $_{CT}$ or $_{ACT}$ treatments) were >97% eGFP$^-$ (Fig. 5c). Excitingly, these studies demonstrate that more advanced bioactive cargos can be easily incorporated during autonomous molecular compilation and the resulting logic-based operations can be performed in the presence of living cells.

Logic-specified localization of proteins autonomously compiled within mammalian cells

Encouraged by our successes in logically specifying protein binding to extracellular membrane components, we next sought to examine whether our method could be used to both autonomously compile and subsequently execute nested Boolean operations within living mammalian cells. In this regard, we looked to logically specify whether an expressed protein would translocate to the interior cell membrane or throughout the cytosol. Taking advantage of our system's genetic encodability, we generated a stable HEK293 cell line by lentivirus transduction that expressed a C∨(T∧V) motif bridging mGreenLantern and a

membrane-binding CAAX motif[72] through an OR/(AND)-gated topology (Fig. 6a and Supplementary Methods); if the correct protease combinations were present, we anticipated that the mGreenLantern cargo would be proteolytically cleaved from the CAAX tag, shuffling it from the membrane to the cytosol. These stably modified cells were subsequently transfected with plasmids that individually encoded for each of the input combinations (that is, $_{N}$, $_{C}$, $_{T}$, $_{V}$, $_{CT}$, $_{CV}$ and $_{CTV}$), where each protease was separated by a self-cleaving P2A peptide sequence[73] and a C-terminal mCherry reporter indicating successful transfection and full plasmid readthrough. Protease-expressing cells were fluorescently imaged by confocal microscopy, with cytosolic mGreenLantern largely confined to the expected input combinations (that is, $_{C}$, $_{CT}$, $_{CV}$, $_{TV}$ and $_{CTV}$) (Fig. 6b). Radial distribution of mGreenLantern was calculated using CellProfiler (25 total bins) throughout individual mCherry^{+} cells from each of the eight treatment conditions. Taking the 'cell membrane' as the outermost 20.8% of these radial bins (5 of 24 total), we quantified the relative amounts of cytosolic mGreenLantern protein throughout the cell (Fig. 6c,d). As programmed, the mGreenLantern remained membrane bound through the intact CAAX motif for $_{N}$, $_{T}$ and $_{V}$ conditions. Notably, some degree of mGreenLantern presented within the cytosol for the $_{T}$ treatment, which we attributed to proteolytic cleavage of the T linkage before SnoopLigation-mediated AND gate formation, thereby removing the CAAX tag from the mGreenLantern protein in these cases; this is not unexpected, given that the proteases and C∨(T∧V) construct are being coexpressed within the same cell. These studies highlight the ability to both autonomously compile and logically dictate protein presentation within mammalian cells, offering exciting potential for cell and tissue engineering applications.

Discussion

In this work, we introduced and harnessed the concept of autonomous macromolecular compilation to create bioactive proteins that can be site-specifically tethered to and conditionally released from biomaterials and cells following user-programmable and hierarchically nested Boolean YES/OR/AND operations. Exploiting the intrinsic modularity and scalability of recombinant expression, we demonstrated multiplexed and multi-stimuli-triggered protein release from biomaterials, including release through a five-input-responsive (AND/(OR))OR(AND)-gated system, as well as the logically defined protein localization on or within living mammalian cells. Our design rules yield species that are structurally simple yet functionally complex, all through direct and unsupervised biosynthesis.

The power of the presented approach lies in its modularity. Although we used five orthogonal proteases to serve as inputs, alternative protease inputs associated with overproduction in disease states could be easily incorporated for natural targeting and cargo release[74]. Additionally, polypeptide motifs that sense and respond to other input types (for example, light[18,75] and small molecules[76]) can be readily incorporated to afford additionally engineered programmability. Moreover, alternative approaches that map nonproteinaceous inputs onto protease function and/or expression could be readily implemented; protease bioactives can be conditionally regulated with alternative inputs (for example, small-molecule-mediated heterodimerization of split protein pairs[77] or direct photoactivation[78]), just as protease expression can be selectively induced (for example, heat-shock promoters, optogenetic activators, small-molecule addition and CRISPRa).

Beyond the fluorescent cargos initially adopted for their ease of characterization, Boolean-actuated release of more functional bioactive proteins (for example, enzymes and growth factors) should be easily attained. While we used SpyTag and Catcher ligation to tether proteins to materials, this chemistry can likely be effortlessly swapped for alternative (non)covalent reactions, including those involving de novo-designed heterodimer interactions[79] or click-type handle installation through genetic code expansion[80]. Lastly, as the systems are fully genetically encoded, additional opportunities exist to both create and functionally deploy these platforms in cellulo and potentially even in vivo. Because of its powerful simplicity and plug-and-play potential, we expect that this approach will find a host of applications in highly targeted drug delivery, on-demand biosensor engineering and next-generation protein architecture development and refinement.

Online content

Any methods, additional references, Nature Portfolio reporting summaries, source data, extended data, supplementary information, acknowledgements, peer review information, details of author contributions, competing interests, and statements of data and code availability are available at https://doi.org/10.1038/s41589-025-02037-5.

References

1. Badeau, B. A. & DeForest, C. A. Programming stimuli-responsive behavior into biomaterials. *Annu. Rev. Biomed. Eng.* **21**, 241–265 (2019).
2. Liu, A. P. et al. The living interface between synthetic biology and biomaterial design. *Nat. Mater.* **21**, 390–397 (2022).
3. Narkar, A. R., Tong, Z., Soman, P. & Henderson, J. H. Smart biomaterial platforms: controlling and being controlled by cells. *Biomaterials* **283**, 121450 (2022).
4. Li, J. & Mooney, D. J. Designing hydrogels for controlled drug delivery. *Nat. Rev. Mater.* **1**, 16071 (2016).
5. Rizzo, F. & Kehr, N. S. Recent advances in injectable hydrogels for controlled and local drug delivery. *Adv. Healthc. Mater.* **10**, 2001341 (2021).
6. Drury, J. L. & Mooney, D. J. Hydrogels for tissue engineering: scaffold design variables and applications. *Biomaterials* **24**, 4337–4351 (2003).
7. Malda, J. et al. 25th anniversary article: engineering hydrogels for biofabrication. *Adv. Mater.* **25**, 5011–5028 (2013).
8. Aisenbrey, E. A. & Murphy, W. L. Synthetic alternatives to Matrigel. *Nat. Rev. Mater.* **5**, 539–551 (2020).
9. Hofer, M. & Lutolf, M. P. Engineering organoids. *Nat. Rev. Mater.* **6**, 402–420 (2021).
10. Johnston, T. G. et al. Compartmentalized microbes and co-cultures in hydrogels for on-demand bioproduction and preservation. *Nat. Commun.* **11**, 563 (2020).
11. Fisher, S. A., Baker, A. E. G. & Shoichet, M. S. Designing peptide and protein modified hydrogels: selecting the optimal conjugation strategy. *J. Am. Chem. Soc.* **139**, 7416–7427 (2017).
12. Shadish, J. A. & DeForest, C. A. Site-selective protein modification: from functionalized proteins to functional biomaterials. *Matter* **2**, 50–77 (2020).
13. Gharios, R., Francis, R. M. & DeForest, C. A. Chemical and biological engineering strategies to make and modify next-generation hydrogel biomaterials. *Matter* **6**, 4195–4244 (2023).
14. Gharios, R., Li, A., Kopyeva, I., Francis, R. M. & DeForest, C. A. One-step purification and N-terminal functionalization of bioactive proteins via atypically split inteins. *Bioconjug. Chem.* **35**, 750–757 (2024).
15. Kloxin, A. M., Kasko, A. M., Salinas, C. N. & Anseth, K. S. Photodegradable hydrogels for dynamic tuning of physical and chemical properties. *Science* **324**, 59–63 (2009).
16. Brown, T. E., Marozas, I. A. & Anseth, K. S. Amplified photodegradation of cell-laden hydrogels via an addition–fragmentation chain transfer reaction. *Adv. Mater.* **29**, 1605001 (2017).
17. Chapla, R., Hammer, J. A. & West, J. L. Adding dynamic biomolecule signaling to hydrogel systems via tethered photolabile cell-adhesive proteins. *ACS Biomater. Sci. Eng.* **8**, 208–217 (2022).

18. Shadish, J. A., Strange, A. C. & DeForest, C. A. Genetically encoded photocleavable linkers for patterned protein release from biomaterials. *J. Am. Chem. Soc.* **141**, 15619–15625 (2019).
19. Kilic Boz, R. et al. Redox-responsive hydrogels for tunable and "on-demand" release of biomacromolecules. *Bioconjug. Chem.* **33**, 839–847 (2022).
20. Lueckgen, A. et al. Enzymatically-degradable alginate hydrogels promote cell spreading and in vivo tissue infiltration. *Biomaterials* **217**, 119294 (2019).
21. Tanimoto, R., Ebara, M. & Uto, K. Tunable enzymatically degradable hydrogels for controlled cargo release with dynamic mechanical properties. *Soft Matter* **19**, 6224–6233 (2023).
22. Ding, H. et al. Preparation and application of pH-responsive drug delivery systems. *J. Control. Release* **348**, 206–238 (2022).
23. Burdick, J. A. & Murphy, W. L. Moving from static to dynamic complexity in hydrogel design. *Nat. Commun.* **3**, 1269 (2012).
24. Zhao, Z., Ukidve, A., Kim, J. & Mitragotri, S. Targeting strategies for tissue-specific drug delivery. *Cell* **181**, 151–167 (2020).
25. Manzari, M. T. et al. Targeted drug delivery strategies for precision medicines. *Nat. Rev. Mater.* **6**, 351–370 (2021).
26. Culver, H. R., Clegg, J. R. & Peppas, N. A. Analyte-responsive hydrogels: intelligent materials for biosensing and drug delivery. *Acc. Chem. Res.* **50**, 170–178 (2017).
27. Herrmann, A., Haag, R. & Schedler, U. Hydrogels and their role in biosensing applications. *Adv. Healthc. Mater.* **10**, 2100062 (2021).
28. Ikeda, M. et al. Installing logic-gate responses to a variety of biological substances in supramolecular hydrogel–enzyme hybrids. *Nat. Chem.* **6**, 511–518 (2014).
29. Hou, B., et al. Engineering stimuli-activatable Boolean logic prodrug nanoparticles for combination cancer immunotherapy. *Adv. Mater.* **32**, 1907210 (2020).
30. Zhang, P. et al. A programmable polymer library that enables the construction of stimuli-responsive nanocarriers containing logic gates. *Nat. Chem.* **12**, 381–390 (2020).
31. Gawade, P. M., Shadish, J. A., Badeau, B. A. & DeForest, C. A. Logic-based delivery of site-specifically modified proteins from environmentally responsive hydrogel biomaterials. *Adv. Mater.* **31**, 1902462 (2019).
32. Ruskowitz, E. R., Comerford, M. P., Badeau, B. A. & DeForest, C. A. Logical stimuli-triggered delivery of small molecules from hydrogel biomaterials. *Biomater. Sci.* **7**, 542–546 (2019).
33. Badeau, B. A., Comerford, M. P., Arakawa, C. K., Shadish, J. A. & DeForest, C. A. Engineered modular biomaterial logic gates for environmentally triggered therapeutic delivery. *Nat. Chem.* **10**, 251–258 (2018).
34. Thompson, R. E. & Muir, T. W. Chemoenzymatic semisynthesis of proteins. *Chem. Rev.* **120**, 3051–3126 (2020).
35. de la Torre, D. & Chin, J. W. Reprogramming the genetic code. *Nat. Rev. Genet.* **22**, 169–184 (2021).
36. Scott, C. P., Abel-Santos, E., Wall, M., Wahnon, D. C. & Benkovic, S. J. Production of cyclic peptides and proteins in vivo. *Proc. Natl Acad. Sci. USA* **96**, 13638–13643 (1999).
37. Iwai, H., Lingel, A. & Plückthun, A. Cyclic green fluorescent protein produced in vivo using an artificially split PI-*Pfu*I intein from *Pyrococcus furiosus*. *J. Biol. Chem.* **276**, 16548–16554 (2001).
38. Zhang, W.-B., Sun, F., Tirrell, D. A. & Arnold, F. H. Controlling macromolecular topology with genetically encoded SpyTag–SpyCatcher chemistry. *J. Am. Chem. Soc.* **135**, 13988–13997 (2013).
39. Schoene, C., Bennett, S. P. & Howarth, M. SpyRings declassified: a blueprint for using isopeptide-mediated cyclization to enhance enzyme thermal resilience. *Methods Enzymol.* **580**, 149–167 (2016).
40. Fan, R. & Aranko, A. S. Catcher/Tag toolbox: biomolecular click-reactions for protein engineering beyond genetics. *ChemBioChem* **25**, e202300600 (2024).
41. Qu, Z., Cheng, S. Z. D. & Zhang, W.-B. Macromolecular topology engineering. *Trends Chem.* **3**, 402–415 (2021).
42. Liu, Y. et al. Mechano-bioconjugation strategy empowering fusion protein therapeutics with aggregation resistance, prolonged circulation, and enhanced antitumor efficacy. *J. Am. Chem. Soc.* **144**, 18387–18396 (2022).
43. Bai, X. et al. Cellular synthesis of protein pretzelanes. *Giant* **10**, 100092 (2022).
44. Hou, B., Yan, X., He, J., Zhang, W.-B. & Shao, Y. Self-assembly of three-component bolaform giant surfactants with branched architectures. *Giant* **15**, 100165 (2023).
45. Snoj, J., Lapenta, F. & Jerala, R. Preorganized cyclic modules facilitate the self-assembly of protein nanostructures. *Chem. Sci.* **15**, 3673–3686 (2024).
46. Bressler, E. M. et al. Boolean logic in synthetic biology and biomaterials: Towards living materials in mammalian cell therapeutics. *Clin. Transl. Med.* **13**, e1244 (2023).
47. Campbell, B. C. et al. mGreenLantern: a bright monomeric fluorescent protein with rapid expression and cell filling properties for neuronal imaging. *Proc. Natl Acad. Sci. USA* **117**, 30710–30721 (2020).
48. Dorr, B. M., Ham, H. O., An, C., Chaikof, E. L. & Liu, D. R. Reprogramming the specificity of sortase enzymes. *Proc. Natl Acad. Sci. USA* **111**, 13343–13348 (2014).
49. Bretherton, R. C., et al. User-controlled 4D biomaterial degradation with substrate-selective sortase transpeptidases for single-cell biology. *Adv. Mater.* **35**, 2209904 (2023).
50. Kopyeva, I., et al. Stepwise stiffening/softening of and cell recovery from reversibly formulated hydrogel interpenetrating networks. *Adv. Mater.* **36**, 2404880 (2024).
51. Keeble, A. H. et al. DogCatcher allows loop-friendly protein–protein ligation. *Cell Chem. Biol.* **29**, 339–350 (2022).
52. Cabrita, L. D. et al. Enhancing the stability and solubility of TEV protease using in silico design. *Protein Sci.* **16**, 2360–2367 (2007).
53. Zakeri, B. et al. Peptide tag forming a rapid covalent bond to a protein, through engineering a bacterial adhesin. *Proc. Natl Acad. Sci. USA* **109**, E690–E697 (2012).
54. Stevens, A. J. et al. Design of a split intein with exceptional protein splicing activity. *J. Am. Chem. Soc.* **138**, 2162–2165 (2016).
55. Thompson, R. E., Stevens, A. J. & Muir, T. W. Protein engineering through tandem transamidation. *Nat. Chem.* **11**, 737–743 (2019).
56. Townend, J. E. & Tavassoli, A. Traceless production of cyclic peptide libraries in *E.coli*. *ACS Chem. Biol.* **11**, 1624–1630 (2016).
57. Veggiani, G. et al. Programmable polyproteams built using twin peptide superglues. *Proc. Natl Acad. Sci. USA* **113**, 1202–1207 (2016).
58. Xu, Q. et al. Catcher/Tag cyclization introduces electrostatic interaction mediated protein–protein interactions to enhance the thermostability of luciferase. *Process Biochem.* **80**, 64–71 (2019).
59. Sun, F. & Zhang, W.-B. Genetically encoded click chemistry. *Chin. J. Chem.* **38**, 894–896 (2020).
60. Evans, T. C., Benner, J. & Xu, M.-Q. The cyclization and polymerization of bacterially expressed proteins using modified self-splicing inteins. *J. Biol. Chem.* **274**, 18359–18363 (1999).
61. Siebold, C. & Erni, B. Intein-mediated cyclization of a soluble and a membrane protein in vivo: function and stability. *Biophys. Chem.* **96**, 163–171 (2002).
62. Qi, X. & Xiong, S. Intein-mediated backbone cyclization of VP1 protein enhanced protection of CVB3-induced viral myocarditis. *Sci. Rep.* **7**, 41485 (2017).

63. Oliveira-Silva, R. et al. Monitoring proteolytic activity in real time: a new world of opportunities for biosensors. *Trends Biochem. Sci.* **45**, 604–618 (2020).
64. Agard, N. J., Prescher, J. A. & Bertozzi, C. R. A strain-promoted [3 + 2] azide–alkyne cycloaddition for covalent modification of biomolecules in living systems. *J. Am. Chem. Soc.* **126**, 15046–15047 (2004).
65. DeForest, C. A., Polizzotti, B. D. & Anseth, K. S. Sequential click reactions for synthesizing and patterning three-dimensional cell microenvironments. *Nat. Mater.* **8**, 659–664 (2009).
66. Nallamsetty, S. et al. Efficient site-specific processing of fusion proteins by tobacco vein mottling virus protease in vivo and in vitro. *Protein Expr. Purif.* **38**, 108–115 (2004).
67. Abdelkader, E. H. & Otting, G. NT*-HRV3CP: an optimized construct of human rhinovirus 14 3C protease for high-yield expression and fast affinity-tag cleavage. *J. Biotechnol.* **325**, 145–151 (2021).
68. Qu, Z. et al. A single-domain green fluorescent protein catenane. *Nat. Commun.* **14**, 3480 (2023).
69. Li, T., Zhang, F., Fang, J., Liu, Y. & Zhang, W.-B. Rational design and cellular synthesis of proteins with unconventional chemical topology. *Chin. J. Chem.* **41**, 2873–2880 (2023).
70. Pruszynski, M., D'Huyvetter, M., Bruchertseifer, F., Morgenstern, A. & Lahoutte, T. Evaluation of an anti-HER2 nanobody labeled with ^{225}Ac for targeted α-particle therapy of cancer. *Mol. Pharm.* **15**, 1457–1466 (2018).
71. Burgstaller, S. et al. Monitoring extracellular ion and metabolite dynamics with recombinant nanobody-fused biosensors. *iScience* **25**, 104907 (2022).
72. Roberts, P. J. et al. Rho family GTPase modification and dependence on CAAX motif-signaled posttranslational modification. *J. Biol. Chem.* **283**, 25150–25163 (2008).
73. Szymczak, A. L. et al. Correction of multi-gene deficiency in vivo using a single 'self-cleaving' 2A peptide-based retroviral vector. *Nat. Biotechnol.* **22**, 589–594 (2004).
74. Vizovišek, M., Fonović, M. & Turk, B. Cysteine cathepsins in extracellular matrix remodeling: extracellular matrix degradation and beyond. *Matrix Biol.* **75–76**, 141–159 (2019).
75. Zhang, W. et al. Optogenetic control with a photocleavable protein, PhoCl. *Nat. Methods* **14**, 391–394 (2017).
76. Dang, B. et al. SNAC-tag for sequence-specific chemical protein cleavage. *Nat. Methods* **16**, 319–322 (2019).
77. Fink, T. et al. Design of fast proteolysis-based signaling and logic circuits in mammalian cells. *Nat. Chem. Biol.* **15**, 115–122 (2019).
78. Nguyen, D. P. et al. Genetic encoding of photocaged cysteine allows photoactivation of TEV protease in live mammalian cells. *J. Am. Chem. Soc.* **136**, 2240–2243 (2014).
79. Chen, Z. et al. Programmable design of orthogonal protein heterodimers. *Nature* **565**, 106–111 (2019).
80. Chin, J. W. Expanding and reprogramming the genetic code. *Nature* **550**, 53–60 (2017).

Methods

Protein expression and purification

All construct plasmids were ordered from GenScript (Piscataway) and made available on Addgene (243769–243798). *E. coli* cells [BL21(DE3) or SHuffle] were transformed with the proper operator plasmid construct and grown at 37 °C for BL21 strains (New England Biolabs, C2527H) or 30 °C for SHuffle strains (New England Biolabs, C3029J) with 220-rpm agitation to an optical density (OD) of 0.6–0.8 in lysogeny broth supplemented with kanamycin. IPTG was used to induce protein expression, at which point the cultures were moved to a reduced temperature (18 °C) for 18 h. Cells were then harvested by centrifugation and either flash-frozen and stored at −80 °C or directly processed for purification.

Standard purification methods were followed. Briefly, cell pellets were reconstituted in lysis buffer (40 ml; 20 mM Tris and 50 mM NaCl, pH 7.5), supplemented with PMSF and sonicated on ice (18 min at 30% amplitude and 33% duty cycle) (Fisher Scientific). Lysates were then centrifuged to separate soluble from insoluble fractions. Clarified lysates were loaded onto an ÄKTA Pure 25-L fast protein LC instrument (Cytiva) equipped with a HisTrap HP column. The HisTrap column was equilibrated with lysis buffer before loading and then the sample was applied. Once all protein was bound, the column was washed with lysis buffer until residual ultraviolet readouts (λ = 280 nm) dropped to 0 absorbance units. Target protein was then eluted off the column into a 96-well plate by switching to elution buffer (lysis buffer + 250 mM imidazole). Eluate fractions were preliminarily assessed for purity by SDS–PAGE; the purest fractions were then pooled pending further dialysis for SEC. Protein yield was determined by measuring pooled elution concentration (NanoDrop2000/2000c 1.6.198, A_{280} absorbance) and then backcalculating the final yield per liter of culture.

For linear constructs that had no higher-order macrocycle contaminants, the pooled purified protein was dialyzed (20 mM Tris and 50 mM NaCl, pH 7.5) to remove imidazole (SnakeSkin dialysis tubing, 10-kDa molecular weight cutoff (MWCO); Fischer Scientific). Proteins were then spun-concentrated if needed using an Amicon Ultra 15 centrifugation filter (10-kDa MWCO; Sigma-Alrich). The purified solution was supplemented with glycerol (10%), aliquoted and flash-frozen with liquid nitrogen before long-term storage at −80 °C.

For cyclized constructs, proteins were loaded onto a HiLoad 26/600 Superdex 75pg SEC column. The column was preequilibrated with a high-salt buffer solution (20 mM Tris and 300 mM NaCl, pH 7.5). Buffer flow rate through the system occurred at 1.5–1.8 ml min^{-1}. Purified eluates were collected in 96-well tubes. Fraction purity was reassessed by SDS–PAGE. Gels were imaged using an Azure 600 AZI600 scanner with Azure Biosystems 1.6.4.1229 software and then gel densitometry was performed in ImageJ 1.53c to determine final sample purity and presence of macrocycles. Final products were spin-concentrated and stocked as previously described.

In-solution treatment and analysis of protein library

Each of the 17 mGreenLantern YES/OR/AND nested protein operators were treated with $2^3 = 8$ possible combinations of inputs emanating from $_{A, S}$ and $_T$. Protease treatments were performed in buffer containing 20 mM Tris and 50 mM NaCl, pH 7.5, supplemented with 1 mM DTT, 1 mM $CaCl_2$, 18 mM GGG and the input-relevant enzymes. Molar ratios of protease to the appropriate mGreenLantern construct were 1:100, 1:100 and 1:10 for $_{A, S}$ and $_T$, respectively. Reaction volumes were adjusted with buffer to compensate for varying volumes of added proteases to equate final protein concentration for gel densitometry. Enzymatic treatments were allowed to proceed for 6 h at 4 °C, with nonkinetically limited endpoints determined to yield full cleavage for all constructs. Reactions were run in triplicate and analyzed by SDS–PAGE. Gel densitometry was then performed using ImageJ 1.53c to determine the normalized percentage of cargo released. Band intensity for the uncleaved and released cargo was determined for each input combination, allowing for the percentage released to be calculated in Microsoft Excel (2016).

Bead release assay for logical operators

Magnetic beads functionalized with DBCO (Vector Laboratories) were preequilibrated in reaction buffer (20 mM Tris and 50 mM NaCl, pH 7.5, supplemented with 1 mM DTT, 1 mM $CaCl_2$ and 18 mM GGG) and washed. Bead washes consisted of diluting the working bead slurry volume (50–100 µl) in 1 ml of reaction buffer. The microcentrifuge tube containing the slurry were placed in a magnetic separation rack to pull the beads toward the tube wall. While tubes were in the slot, fresh reaction buffer was added and the solution was mixed before additional washes using the same method (>5 times). After equilibration, beads were reacted with SpyCatcher-azide for 2 h at room temperature on a tube rotator and mixer. Beads were again washed as described before removing unbound SpyCatcher-azide. The appropriate SpyTagged operator was then added to conjugate onto the beads through SpyLigation. Reactions were kept in a tube rotator and mixer for 2 h at room temperature before thorough washing to remove any unbound mGreenLantern.

All eight possible input combinations of $_{A, S}$ and $_T$ had molar ratios of protease to each mGreenLantern (assumed to have conjugated onto the beads at 50% efficiency) construct of 1:100, 1:100 and 1:10 for $_{A, S}$ and $_T$, respectively. Treatments were performed for 6 h at 4 °C. Afterward, 15 µL was taken from each input condition with a gel-loading pipette and added to a clear-bottom 384-well black plate. Supernatant fluorescence measurements were taken on a BioTek Synergy microplate reader (BioTek; Gen5 version 3.09 software). All conditions were performed in at least three technical triplicates. Fluorescence measurements were normalized by calculating the average fluorescence per input and then the percentage of cargo released was calculated assuming that the brightest fluorescence measurement was 100% released.

Multiplexed release from polymeric hydrogels

Hydrogels were formulated from PEG-tetraBCN ($M_n \approx 20{,}000$ Da, 4 mM), TEG diazide (MW = 200.2 g mol^{-1}, 8 mM), SpyCatcher-azide (15 µM) and the set of SpyTagged fluorescent proteins (2 µM each) in gel buffer (20 mM Tris, 50 mM NaCl and 10 mM $CaCl_2$, pH 7.5). The fluorescent protein constructs and SpyCatcher-azide were first reacted before the addition of PEG-tetraBCN. Then TEG-diazide was added and the mixture was aliquoted into microcentrifuge tubes (1.5 ml), where the materials formed hydrogels. Gel buffer was added to each tube and the formed hydrogels were washed for 72 h with three buffer changes to remove unconjugated fluorescent protein. Depending on the intended input, samples were treated with a combination of $_{A, S}$ and $_T$ at concentrations of 5 µM, 5 µM and 7 µM, respectively. All treatments were performed at 4 °C in gel buffer supplemented with DTT (1 mM) for 6 h. Supernatant fluorescence was measured and used to calculate the corresponding concentrations of released mGreenLantern, mCherry and mCerulean proteins. Fluorescence normalization was performed as previously stated in the bead release assay method.

Extracellular membrane labeling with HER2Nb–eGFP

HER2Nb-C∧(A∨T)–SpyTag and eGFP–SpyCatcher were expressed and purified as previously described, with the addition of an endotoxin wash (standard lysis buffer supplemented with 0.1% Triton X-114). HER2Nb–SpyTag and eGFP–SpyCatcher were reacted at a 1:1 molar ratio for 14–16 h at 4 °C on a rocker. The HER2Nb now tagged with eGFP (denoted HER2Nb-C∧(A∨T)–eGFP) was supplemented with 1 mM DTT, 1 mM $CaCl_2$ and 18 mM GGG and then treated with $2^3 = 8$ possible combinations of inputs emanating from $_{A, C}$ and $_T$. Molar ratios of protease added were 1:100, 1:50 and 1:50 for $_{A, C}$ and $_T$, respectively. Enzymatic treatments were allowed to proceed for 6 h at 4 °C, with nonkinetically limited endpoints determined to yield full cleavage for all constructs. Protease-treated samples were then used for SDS–PAGE analysis or membrane-labeling experiments.

To image membrane labeling of SK-BR-3 breast cancer cells overexpressing HER2 receptors (HTB-30, American Type Culture Collection (ATCC)), cells were seeded overnight on an eight-chamber glass slide (ibidi) in DMEM supplemented with 1% penicillin–streptomycin and 10% FBS. The wells were washed once with cold PBS; then, 100 nM protease-treated HER2Nb-C∧(A∨T)–eGFP and 1:1,500 dilution of Hoechst 33342 in PBS was incubated with the cells for 1 h at 4 °C. The cells were washed twice with cold PBS and then imaged on a Leica Stellaris 5 confocal microscope (Leica; Leica Application Suite X 4.5.0.25531) at ×10 magnification.

For flow cytometry, SK-BR-3 cells were passaged and resuspended at 1×10^6 cells per ml in fluorescence-activated cell sorting (FACS) buffer (PBS and 1% BSA). The cells were washed once with cold FACS buffer; then, 100 nM protease-treated HER2Nb-C∧(A∨T)–eGFP in FACS buffer was incubated with the cells for 1 h at 4 °C. The cells were washed twice with cold FACS buffer and eGFP-positive events were collected on a BD FACSSymphony A3 analyzer (BD Bioscience; BD FACSDiva version 8.0 software). Data were analyzed in FlowJo version 10 to determine the percentage of the population positive for eGFP.

Intracellular Boolean logic membrane labeling

A stable HEK293T cell line (CRL-3216, ATCC) that continuously expresses mGreenLantern-C∧(T∨V)–CAAX was produced. Briefly, HEKs were transfected with envelope plasmid pMD2.G (Addgene, 12259), packaging plasmids pMDLG/pRRE (Addgene, 12251) and pRSV-REV (Addgene, 12253) and the mGreenLantern-C∧(T∨V)–CAAX using Lipofectamine 2000 (Invitrogen). Cells were cultured for 2 days after transfection and virus-laden medium was isolated. Active lentivirus was concentrated by mixing viral medium with 4× lentiviral concentration solution (40% w/v PEG-8000 and 1.2 M NaCl), and incubated overnight at 4 °C. Flocculated lentiviral particles were pelleted, resuspended at 10× in PBS and then stored at −80 °C until use.

Fresh HEK293T cells were plated in a 35-mm dish (Fisher Scientific). After allowing the cells to adhere, the medium was supplemented with concentrated lentivirus and incubated overnight. The following day, mGreenLantern production was confirmed by confocal microscopy (Leica; Leica Application Suite X 4.5.0.25531). Cells were selected in 10 μg ml^{-1} puromycin (Fisher Scientific) for 24 h and then DMEM was replaced; the surviving transgenic cells were allowed to recover and expand. mGreenLantern expression was optimized later by fluorescence assisted cell sorting on a Symphony A6 (BD BioSciences).

Protease treatment was performed by transient transfection of plasmids containing protease(s) on a polycistronic expression cassette with a C-terminally expressed mCherry cassette to assay transfection efficiency. mGreenLantern expressing HEK293T cells were transfected with Lipofectamine 3000 (Invitrogen) and allowed to recover for 24 h. Cells were then imaged using confocal microscopy (Leica) and saved images were cropped such that one cell expressing both mGreenLantern and mCherry was present per image. Single-cell images were processed using CellProfiler 4.2.1. Regions of interest were manually determined and the membrane or cytosolic localization of mGreenLantern was reported as a radial distribution function relative to the center of a cell-containing region of interest. The outermost 20.8% of the object was considered to be the membrane and the interior remainder was considered to be the cytosol.

Statistical Analysis

Statistical tests and graphs were completed in GraphPad Prism (version 6). All data presented were from experiments performed in triplicate, with plots displaying the mean ± 1 s.d. about the mean, unless otherwise stated.

Reporting summary

Further information on research design is available in the Nature Portfolio Reporting Summary linked to this article.

Data availability

All pertinent experimental and characterization data are available within this paper and its associated Supplementary Information. Plasmids generated during the current study are listed in the Supplementary Information and are available through Addgene. Source data are provided with this paper.

Acknowledgements

We thank R. Francis and A. Garcia for collaborating on designing and validating the SpyCatcher-azide, C. Yang and R. Brady for synthesizing and supplying PEG-tetraBCN and J. Davis for gifting HEK293T cells (previously obtained from the ATCC, CRL-3216). We acknowledge support from D. Whittington at the University of Washington MS Center. Part of this work was conducted with instrumentation provided by the Joint Center for Deployment and Research in Earth Abundant Materials. This work was supported by a grant (DMR 1807398, C.A.D.) from the National Science Foundation and a Maximizing Investigators' Research Award (R35GM138036, C.A.D.) from the National Institutes of Health. Student support was further provided through a John C. Berg Endowed Fellowship (R.G.), the National Science Foundation (DGE-2140004, M.L.R.), a Goldwater Scholarship (A.L.), a Washington NASA Space Grant (A.L), a University of Washington MEM-C Academic-Year Research Accelerator Fellowship (A.L) and a University of Washington Mary Gates Endowment for Students (S.P.K.).

Author contributions

R.G., M.L.R., and C.A.D. conceptualized and designed the experiments. R.G., M.L.R., A.L., S.P.K. and J.H. performed the experiments. R.G., M.L.R., A.L., S.P.K., J.H. and C.A.D. analyzed the data. C.A.D. prepared the main text figures with input from R.G. and M.L.R. C.A.D. and M.L.R. prepared the supplementary figures with input from R.G. R.G., M.L.R. and C.A.D. wrote the paper with input from all other authors.

Competing interests

C.A.D., R.G. and M.L.R. have filed a patent application (PCT/US2025/031504) related to the work described in this article. The other authors declare no competing interests.

Additional information

Extended data is available for this paper at https://doi.org/10.1038/s41589-025-02037-5.

Supplementary information The online version contains supplementary material available at https://doi.org/10.1038/s41589-025-02037-5.

Correspondence and requests for materials should be addressed to Cole A. DeForest.

Peer review information *Nature Chemical Biology* thanks Karthik Raman, Laura Sabio, Manuel Salmeron-Sanchez and the other, anonymous reviewer(s) for their contribution to the peer review of this work.

https://doi.org/10.1038/s41589-025-02037-5

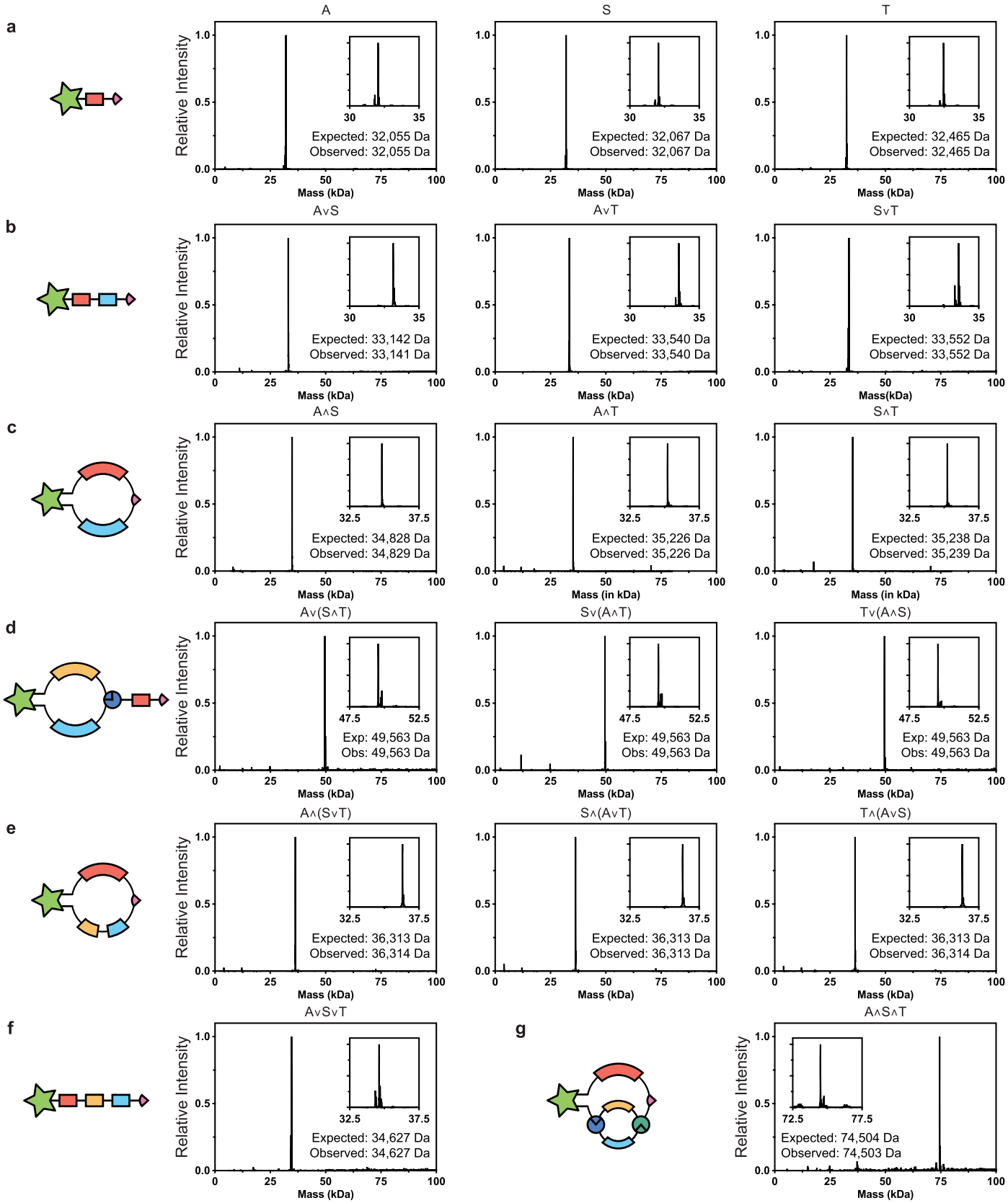

Extended Data Fig. 1 | Mass spectrometric validation of logically releasable mGreenLantern. a, YES-gated single-input tethers. **b-c**, Two-input (b) OR-gated and (c) AND-gated tethers. **d-g**, Three-input (d) OR/(AND)-, (e) AND/(OR)-, (f) OR/OR-, and (g) AND/AND-gated tethers. Plot titles correspond to the protein tether identity.

https://doi.org/10.1038/s41589-025-02037-5

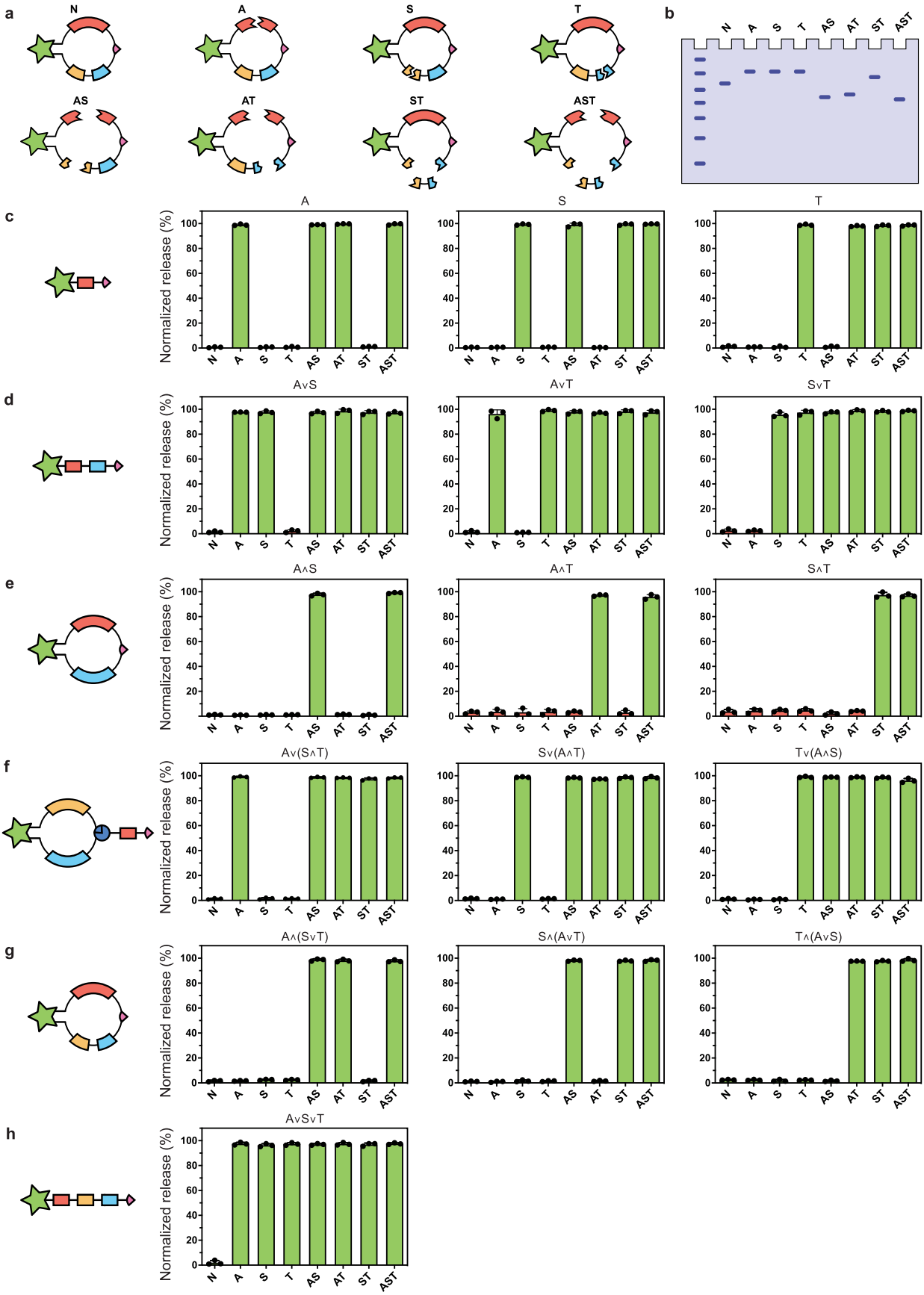

Extended Data Fig. 2 | See next page for caption.

https://doi.org/10.1038/s41589-025-02037-5

Extended Data Fig. 2 | SDS-PAGE analysis of in-solution treatment of autonomously compiled mGreenLantern pendants. a, mGreenLantern-A∧(S∨T) is differentially cleaved following the 8 possible input combinations of $_{A}$, $_{S}$, and $_{T}$. Input conditions $_{A}$, $_{S}$, $_{T}$, and $_{ST}$ are expected to linearize the product but not induce payload release, leading to a product with less electrophoretic mobility than the initial cyclic construct. Payload release is expected following input conditions $_{AS}$, $_{AT}$, and $_{AST}$, accompanied with a product band that migrates further than the starting species. **b**, Changes in topology and/or molecular weight in response to a specific set of inputs leads to changes in protein electrophoretic mobility, which can be analyzed through gel densitometry. **c**, The response profiles of the YES-gated single-input tethers. **d**-**e**, The response profiles of the two-input (d) OR-gated and (e) AND-gated tethers. **f**-**h**, The response profiles of the three-input (f) OR/(AND)-, (g) AND/(OR)-, and (h) OR/OR-gated tethers. Plot titles correspond to the protein tether identity; the y-axis represents extent of cleavage as measured through migration on an SDS-PAGE with gel densitometry analysis; the x-axis indicates treatment conditions, wherein $_{N}$ indicates no treatment, $_{A}$ indicates eSrtA(2A9), $_{S}$ indicates eSrtA(4S9), and $_{T}$ indicates TEV. Green bars indicate conditions expected to yield tether cleavage, whereas red bars indicate conditions expected to keep the tether non-cleaved. Error bars correspond to ±1 standard deviation about the mean with propagated uncertainties for n = 3 experimental replicates.

https://doi.org/10.1038/s41589-025-02037-5

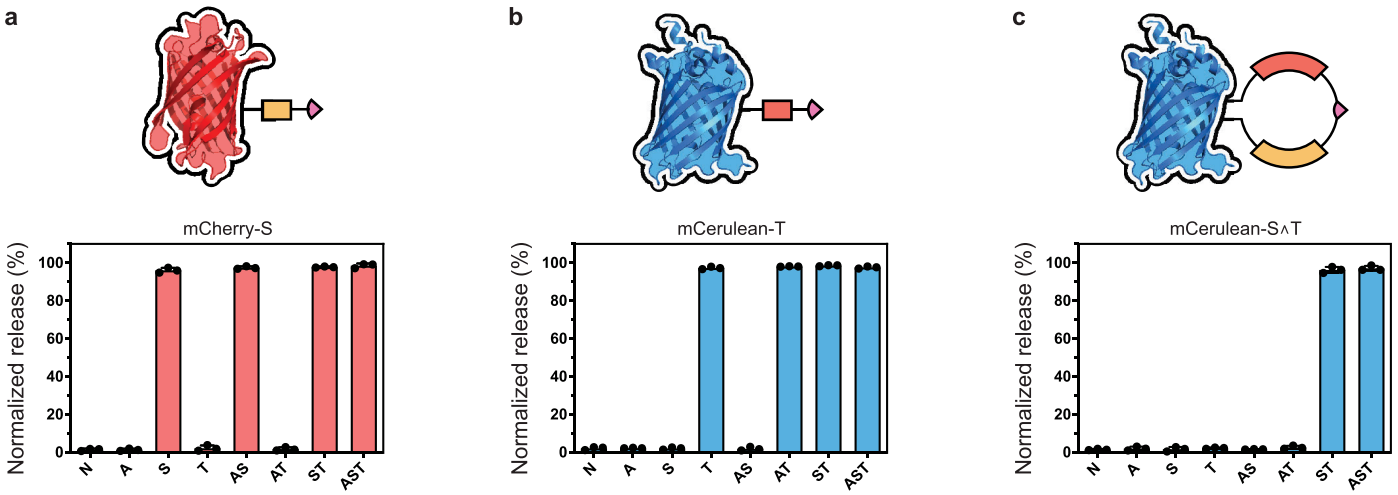

Extended Data Fig. 3 | SDS-PAGE analysis of in-solution treatment of autonomously compiled mCherry and mCerulean pendants. a-c, Changes in topology and/or molecular weight in response to a specific set of inputs leads to changes in protein electrophoretic mobility, which can be analyzed through gel densitometry. Results are shown for species (a) mCherry-S, (b) mCerulean-T, and (c) mCerulean-S∧T. Plot titles correspond to the protein tether identity; the y-axis represents extent of cleavage as measured through migration on an SDS-PAGE with gel densitometry analysis; the x-axis indicates treatment conditions, wherein $_N$ indicates no treatment, $_A$ indicates eSrtA(2A9), $_S$ indicates eSrtA(4S9), and $_T$ indicates TEV. Error bars correspond to ±1 standard deviation about the mean with propagated uncertainties for n = 3 experimental replicates.

https://doi.org/10.1038/s41589-025-02037-5

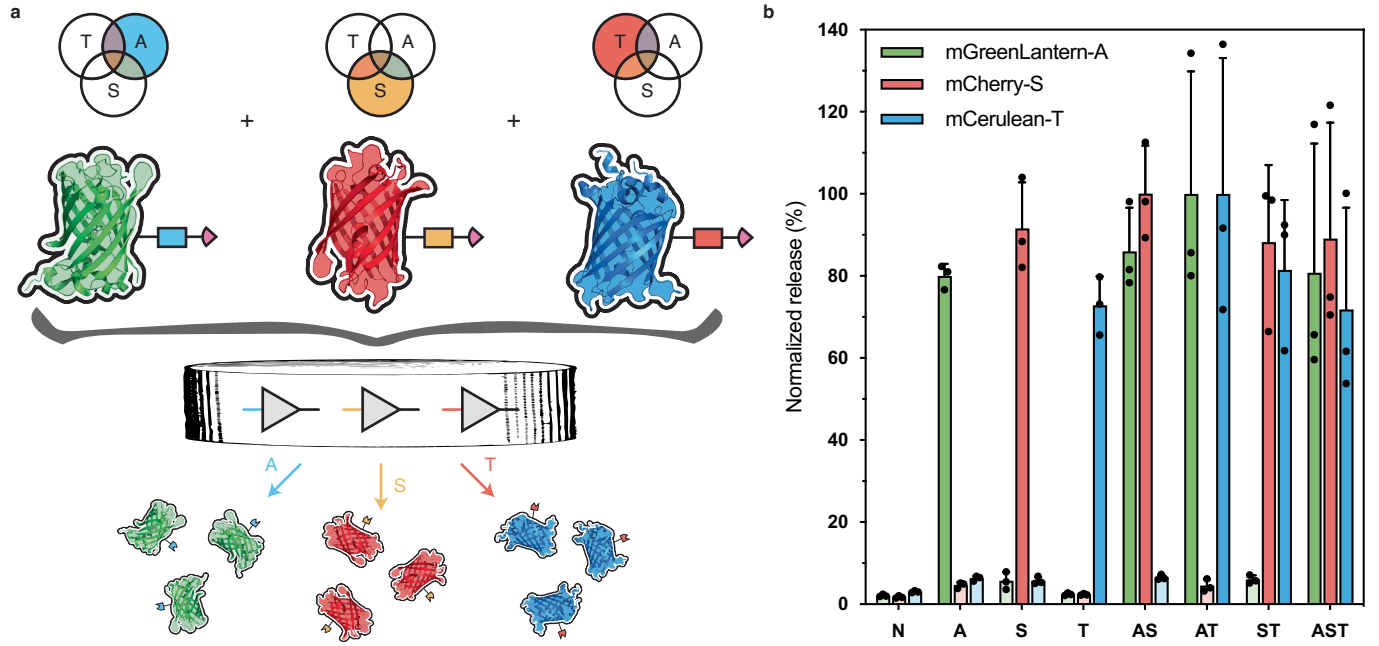

Extended Data Fig. 4 | Multiplexed YES-gated release of proteins from hydrogel biomaterials. a, mGreenLantern-A, mCherry-S, and mCerulean-T are tethered homogenously into an underlying PEG-based hydrogel network via SpyLigation, each exhibiting a different YES-gated response. **b**, Appropriate proteins are individually released when their corresponding input is present. Fully colored bars (green for mGreenLantern, red for mCherry, blue for mCerulean) indicate conditions expected to yield protein release, whereas opaque colored bars denote conditions not expected to result in release. Error bars correspond to ±1 standard deviation about the mean with propagated uncertainties for n = 3 experimental replicates.

nature portfolio

Corresponding author(s): Cole A. DeForest

Last updated by author(s): Sep 4, 2025

Reporting Summary

Nature Portfolio wishes to improve the reproducibility of the work that we publish. This form provides structure for consistency and transparency in reporting. For further information on Nature Portfolio policies, see our Editorial Policies and the Editorial Policy Checklist.

Statistics

For all statistical analyses, confirm that the following items are present in the figure legend, table legend, main text, or Methods section.

n/a	Confirmed
☐	☒ The exact sample size (*n*) for each experimental group/condition, given as a discrete number and unit of measurement
☐	☒ A statement on whether measurements were taken from distinct samples or whether the same sample was measured repeatedly
☒	☐ The statistical test(s) used AND whether they are one- or two-sided *Only common tests should be described solely by name; describe more complex techniques in the Methods section.*
☒	☐ A description of all covariates tested
☒	☐ A description of any assumptions or corrections, such as tests of normality and adjustment for multiple comparisons
☐	☒ A full description of the statistical parameters including central tendency (e.g. means) or other basic estimates (e.g. regression coefficient) AND variation (e.g. standard deviation) or associated estimates of uncertainty (e.g. confidence intervals)
☒	☐ For null hypothesis testing, the test statistic (e.g. *F*, *t*, *r*) with confidence intervals, effect sizes, degrees of freedom and *P* value noted *Give P values as exact values whenever suitable.*
☒	☐ For Bayesian analysis, information on the choice of priors and Markov chain Monte Carlo settings
☒	☐ For hierarchical and complex designs, identification of the appropriate level for tests and full reporting of outcomes
☒	☐ Estimates of effect sizes (e.g. Cohen's *d*, Pearson's *r*), indicating how they were calculated

Our web collection on statistics for biologists contains articles on many of the points above.

Software and code

Policy information about availability of computer code

Data collection	Data collection was performed with the assistance of NanoDrop2000/2000c 1.6.198, Gen5 v3.09, Azure Biosystems 1.6.4.1229, BD FACSDiva v8.0, Leica Application Suite X 4.5.0.25531, and Analyst TF 1.7.1.
Data analysis	Data analysis was performed with the assistance of Microsoft Excel 2016, GraphPad Prism v6, ImageJ 1.53c, Adobe Illustrator CS6 v16.0.0, FlowJo v10, CellProfiler 4.2.1, ChemDraw 20.0, and Peak View 2.2.

For manuscripts utilizing custom algorithms or software that are central to the research but not yet described in published literature, software must be made available to editors and reviewers. We strongly encourage code deposition in a community repository (e.g. GitHub). See the Nature Portfolio guidelines for submitting code & software for further information.

Data

Policy information about availability of data

All manuscripts must include a data availability statement. This statement should provide the following information, where applicable:

- Accession codes, unique identifiers, or web links for publicly available datasets
- A description of any restrictions on data availability
- For clinical datasets or third party data, please ensure that the statement adheres to our policy

All pertinent experimental and characterization data are available within this manuscript and its associated Supplementary Information. Source data is provided with this paper. Plasmids generated during the current study are listed in the Supplementary Information and are available through Addgene.

Research involving human participants, their data, or biological material

Policy information about studies with human participants or human data. See also policy information about sex, gender (identity/presentation), and sexual orientation and race, ethnicity and racism.

Reporting on sex and gender	*Use the terms sex (biological attribute) and gender (shaped by social and cultural circumstances) carefully in order to avoid confusing both terms. Indicate if findings apply to only one sex or gender; describe whether sex and gender were considered in study design; whether sex and/or gender was determined based on self-reporting or assigned and methods used.* *Provide in the source data disaggregated sex and gender data, where this information has been collected, and if consent has been obtained for sharing of individual-level data; provide overall numbers in this Reporting Summary. Please state if this information has not been collected.* *Report sex- and gender-based analyses where performed, justify reasons for lack of sex- and gender-based analysis.*
Reporting on race, ethnicity, or other socially relevant groupings	*Please specify the socially constructed or socially relevant categorization variable(s) used in your manuscript and explain why they were used. Please note that such variables should not be used as proxies for other socially constructed/relevant variables (for example, race or ethnicity should not be used as a proxy for socioeconomic status).* *Provide clear definitions of the relevant terms used, how they were provided (by the participants/respondents, the researchers, or third parties), and the method(s) used to classify people into the different categories (e.g. self-report, census or administrative data, social media data, etc.)* *Please provide details about how you controlled for confounding variables in your analyses.*
Population characteristics	*Describe the covariate-relevant population characteristics of the human research participants (e.g. age, genotypic information, past and current diagnosis and treatment categories). If you filled out the behavioural & social sciences study design questions and have nothing to add here, write "See above."*
Recruitment	*Describe how participants were recruited. Outline any potential self-selection bias or other biases that may be present and how these are likely to impact results.*
Ethics oversight	*Identify the organization(s) that approved the study protocol.*

Note that full information on the approval of the study protocol must also be provided in the manuscript.

Field-specific reporting

Please select the one below that is the best fit for your research. If you are not sure, read the appropriate sections before making your selection.

☒ Life sciences ☐ Behavioural & social sciences ☐ Ecological, evolutionary & environmental sciences

For a reference copy of the document with all sections, see nature.com/documents/nr-reporting-summary-flat.pdf

Life sciences study design

All studies must disclose on these points even when the disclosure is negative.

Sample size	All experiments were performed in triplicate unless otherwise stated. No statistical methods were used to determine sample size. Sufficient microscopy images were collected to ensure their representation of the samples.
Data exclusions	No data was excluded.
Replication	Multiple independent experiments were performed and replicate numbers are stated in the figure captions.
Randomization	Randomization was not required for the experiments performed. Positive and negative controls were utilized when necessary.
Blinding	Blinding was not relevant to the study as there were no participants or relevant biases.

Reporting for specific materials, systems and methods

We require information from authors about some types of materials, experimental systems and methods used in many studies. Here, indicate whether each material, system or method listed is relevant to your study. If you are not sure if a list item applies to your research, read the appropriate section before selecting a response.

Materials & experimental systems

n/a	Involved in the study
☒	☐ Antibodies
☐	☒ Eukaryotic cell lines
☒	☐ Palaeontology and archaeology
☒	☐ Animals and other organisms
☒	☐ Clinical data
☒	☐ Dual use research of concern
☒	☐ Plants

Methods

n/a	Involved in the study
☒	☐ ChIP-seq
☐	☒ Flow cytometry
☒	☐ MRI-based neuroimaging

Eukaryotic cell lines

Policy information about cell lines and Sex and Gender in Research

Cell line source(s)	HEK-293T cells were gifted by Dr. Jennifer Davis (University of Washington), who previously obtained the cells from ATCC (CRL-3216). SK-BR-3 cells were acquired from ATCC (HTB-30).
Authentication	The cell lines were used without further authentication. Genetically modified cell lines clearly exhibited the expected expression and followed appropriate logic operation.
Mycoplasma contamination	Cell lines used were not tested for mycoplasma contamination.
Commonly misidentified lines (See ICLAC register)	HEK cells were used for their ease of transfection. SK-BR-3 cells were used due to their over expression of the HER2 receptor.

Plants

Seed stocks	*Report on the source of all seed stocks or other plant material used. If applicable, state the seed stock centre and catalogue number. If plant specimens were collected from the field, describe the collection location, date and sampling procedures.*
Novel plant genotypes	*Describe the methods by which all novel plant genotypes were produced. This includes those generated by transgenic approaches, gene editing, chemical/radiation-based mutagenesis and hybridization. For transgenic lines, describe the transformation method, the number of independent lines analyzed and the generation upon which experiments were performed. For gene-edited lines, describe the editor used, the endogenous sequence targeted for editing, the targeting guide RNA sequence (if applicable) and how the editor was applied.*
Authentication	*Describe any authentication procedures for each seed stock used or novel genotype generated. Describe any experiments used to assess the effect of a mutation and, where applicable, how potential secondary effects (e.g. second site T-DNA insertions, mosiacism, off-target gene editing) were examined.*

Flow Cytometry

Plots

Confirm that:

☒ The axis labels state the marker and fluorochrome used (e.g. CD4-FITC).

☒ The axis scales are clearly visible. Include numbers along axes only for bottom left plot of group (a 'group' is an analysis of identical markers).

☒ All plots are contour plots with outliers or pseudocolor plots.

☒ A numerical value for number of cells or percentage (with statistics) is provided.

Methodology

Sample preparation	SK-BR-3 cells were resuspended at 1x10^6 cells/mL in Fluorescence-activated cell sorting (FACS) buffer (PBS, 1% BSA). The cells were washed once with cold FACS buffer, then 100mM of protease treated HER2Nb-eGFP in FACS buffer was incubated with the cells for 1 hour at 4°C. The cells were washed twice with cold FACS buffer, then eGFP positive events were counted.
Instrument	BD FACSSymphony A3 analyzer
Software	Data was collected on BD FACSDiva v8.0 and analyzed on FlowJo v10.
Cell population abundance	Flow cytometry was used to quantify extracellular membrane labeling from a HER2 nanobody- eGFP conjugate where cells that did not receive the correct logical inputs remained fluorescent, while those with the correct inputs lost fluorescence.
Gating strategy	Cells were first gated to include only live cells (FSC-A vs. SSC-A). This cell population was then gated to remove doublets (FSC-

Gating strategy

A vs. FSC-H). Further, the cell population was then analyzed for the percent of positive eGFP labeled cells. The eGFP+ threshold was 1.5 x 10^3 AFU.

☒ Tick this box to confirm that a figure exemplifying the gating strategy is provided in the Supplementary Information.